The metamorphic and magmatic record of collisional orogens

Owen M. Weller[1]✉, Catherine M. Mottram[2]✉, Marc R. St-Onge[3], Charlotte Möller[4], Rob Strachan[2], Toby Rivers[5] and Alex Copley[6]

Abstract | The Cenozoic Himalaya-Tibet orogen is generally regarded as the archetypal continental collision zone and is often used as an analogue for interpreting ancient orogenic events. However, given the wide diversity observed in present-day collisional mountain belts, the extent to which such inferences can be made remains debated. In this Review, we compare the metamorphic and magmatic record of the Himalaya-Tibet orogen to four ancient orogens — the Palaeozoic Caledonian orogen, the Meso-Neoproterozoic Grenville and Sveconorwegian orogens, and the Palaeoproterozoic Trans-Hudson orogen — to establish the controls on the underlying dynamics and the nature of the resulting rock record. The similarities in rock records, and, thus, thermal conditions, are interpreted to result from comparable foreland strengths, resulting in similar maximum crustal thicknesses. Apparent differences in the records are mainly attributed to variation in exposed structural level rather than fundamentally different tectonic processes. We, therefore, suggest that foreland rheology is a critical factor in determining the effectiveness of orogen comparisons. Future research is required to investigate the causes and consequences of lateral variability in mountain belts, in particular, focussing on the record of orogens smaller than those considered here, and to understand if and why mountain building processes have varied through Earth history.

[1]Department of Earth Sciences, University of Cambridge, Cambridge, UK.
[2]School of the Environment, Geography and Geosciences, University of Portsmouth, Portsmouth, UK.
[3]Geological Survey of Canada, Ottawa, ON, Canada.
[4]Department of Geology, Lund University, Lund, Sweden.
[5]Department of Earth Sciences, Memorial University of Newfoundland, St. John's, NL, Canada.
[6]COMET, Department of Earth Sciences, University of Cambridge, Cambridge, UK.
✉e-mail: ow212@cam.ac.uk; catherine.mottram@port.ac.uk

https://doi.org/10.1038/s43017-021-00218-z

Continent–continent collisions are among the most spectacular manifestations of tectonics, yielding the highest and most rugged topography on Earth, and playing an important role in modulating climate[1,2], controlling seismic hazard[3,4] and influencing the global carbon cycle[5]. However, the wide deformation zones that characterize continental collisions are not well accounted for by plate tectonics, which describes the motion of rigid plates separated by narrow boundaries[6], and there remains much to be learned about the underlying geodynamic processes of continental collisions.

A crucial data source that can help constrain these geodynamic processes is metamorphic and magmatic rocks produced during continental collision, as these rock types capture fragments of the evolving pressure–temperature–time–deformation (P–T–t–D) conditions associated with mountain building (BOX 1). Advances in phase equilibria modelling[7], petrochronology[8] and structural analysis[9] have allowed P–T–t–D records to be deciphered with increasing precision and accuracy, informing geodynamic models and providing insights into tectonic processes. Together with geophysical observations of active mountain belts[10–13], an understanding of the evolution and behaviour of continent–continent collisions is emerging (FIG. 1).

The ongoing India–Asia collision, which led to the formation of the Himalayan mountain range and the Tibetan plateau (hereafter, the Himalaya-Tibet orogen (HTO)), has been extremely influential in developing understanding of collisional orogens. The HTO constitutes the largest active continental collision zone and its tectonic evolution can be documented in 4D (through space and time). The HTO has been the subject of sustained multidisciplinary study[10–16], resulting in it becoming the classic comparator for similarly sized ancient orogens. Generally, all that remains of these ancient orogens today are their deeply exhumed roots, which, in turn, provide direct access to structural levels not currently exposed in the HTO and give insight into crustal processes at various depths.

However, questions remain regarding the relationship between modern-day HTO and ancient orogens preserved in the rock record, based upon how representative the HTO is of mountain building processes in general. Therefore, it is worthwhile to compare and contrast what is currently known about ancient and modern collisional orogens to continue to develop an understanding of the factors that control mountain building and the nature of the resulting rock record. In turn, this approach allows us to infer possible observational and preservational biases regarding the orogenic rock record.

Key points

- The metamorphic and magmatic rock record of five major orogens — Himalaya-Tibet, Caledonian, Grenville, Sveconorwegian and Trans-Hudson — are compared.
- Commonalities include pre-collisional accretionary tectonics and magmatism, and post-collisional continental underthrusting, crustal thickening and associated metamorphism.
- The post-collisional commonalities are likely to be due to similarities in the strengths of the plates bounding the mountain belts supporting similar crustal thicknesses.
- Differences include the dominant metamorphic grade exposed at the present erosion surface and the preservation of high-pressure and low-temperature rocks.
- The causes of these differences are mainly attributed to contrasts in exposed structural level, rather than differences in the underlying tectonic processes.

Phase equilibria modelling
A method of calculating the pressure and temperature conditions at which a set of minerals (phases) is in equilibrium within a model system.

In this Review, we compare the metamorphic and magmatic rock record of the HTO with a series of collisional orogens that are documented to have been Himalayan-Tibetan in scale. To make the selection temporally representative, we consider mountain belts from each of the three past supercontinent cycles: the Palaeozoic Caledonian orogen (CO) for Pangaea, the Meso-Neoproterozoic Grenville–Sveconorwegian orogenic belt for Rodinia and the Palaeoproterozoic Trans-Hudson orogen (THO) for Nuna[17]. We then summarize the similarities and differences between the records for the five orogens, making inferences regarding the tectonic processes related to orogen formation.

Box 1 | Useful principles

Mountain building (orogenesis) leads to a complex evolution in the pressure–temperature (*P*–*T*) structure of the lithosphere. Pressure can be linked to depth via the relation, $P = \rho g z$, where ρ = density, g = gravity and z = depth. The SI unit for pressure is the Pascal (Pa), but metamorphic pressures are commonly quoted in kilobars, whereby 1 kbar = 10^8 Pa. For a typical crustal rock density of 2,900 kg m^{-3}, 1 kbar = 3.5 km. This relation can be applied to determine the approximate depths of quoted metamorphic pressures.

The evolving temperature–depth structure (known as the geotherm) in mountain belts leads to a wide range of *P*–*T* paths being transiently possible for a given rock, depending on when and where a rock enters the orogenic cycle (FIG. 1). The *P*–*T* changes experienced by a rock induce metamorphic reactions and the formation of new, stable mineral assemblages, which typically 'freeze-in' and record close to the maximum-*T* conditions experienced by the rock during its *P*–*T* path. As certain regions of *P*–*T* space are relatively diagnostic of tectonic settings (for example, low-*T* and high-*P* conditions can only be reached in subduction zone settings), the type and/or spatial distribution of metamorphic rocks can provide a guide to past tectonic settings, as well as providing snapshots of the thermal history.

Where the *P*–*T* conditions exceed the solidus (whose location is dependent on rock composition and particularly sensitive to water content), rocks partially melt and igneous rocks are formed. The composition of igneous rocks is also relatively diagnostic of the setting in which they formed (for example, leucogranites typically form as the product of partial melting in a crustal setting).

Coupled with geochronological and structural analysis to provide further context, the study of metamorphic and igneous rocks, therefore, provides a means to decode the history of an orogen. However, given the broad length scales (up to thousands of kilometres) and timescales (up to hundreds of millions of years) of orogens, the diversity of possible rock types, the complex evolution in thermal structure and the variable preservation, reworking and erosion level, this task is not straightforward. Therefore, to assist in the identification of general principles governing orogen evolution, the metamorphic rocks are grouped into four broad categories based on peak *P*–*T* conditions experienced (FIGS 1,2) and the igneous rocks are generalized into four groups based on inferred melt source region.

Note that, as a further means of trying to compile observations across mountain belts, a nomenclature has evolved that defines metamorphic stages as M1, M2, M3, and so on. These terms represent distinct times and styles of metamorphism in different locations of an orogen, which may be correlated with specific deformation (D) events, but are not, themselves, comparable between orogens.

A reference frame for the comparison

In the next sections, the orogenic belts are reviewed in chronological order (from youngest to oldest). The metamorphic and magmatic features described in these sections are shown in FIG. 2, which displays the orogens in order of average exposed structural level (from shallowest to deepest) (FIG. 1c) and should be referred to throughout the remainder of the paper. The data are described in detail below, but grouped into eight broad categories on FIG. 2. based on peak metamorphic conditions and melt source regions, to aid large-scale comparisons (BOX 1; FIG. 1). To provide a common reference frame, the data in FIG. 2 are aligned using the onset of terminal collision as a common datum (dashed grey line, FIG. 2). Discussion regarding the uncertainty on the timing of collision for each orogen (blue shading, FIG. 2) is given below.

The observations for each orogen are principally divided between units on either side of the collisional suture. In general, one side of the suture has experienced a protracted history of terrane accretion and subduction-related magmatism (for example, Asia in the HTO), whereas the other is characterized by a quiescent history in the lead-up to collision, due to being attached to a subducting oceanic plate (for example, India in the HTO). These two elements could be referred to as the collisional upper and lower plates. However, in all significantly sized orogens, there is overthrusting of a pervasively deformed (so not plate-like) region, onto both of the bounding crustal blocks. Therefore, to better capture the distributed nature of the deformation, this Review mainly distinguishes between the deformation belt and the bounding rigid crustal blocks[6]. This distinction also avoids potential nomenclature problems related to where subduction polarity is not known and/or an orogen is poorly preserved or exposed.

The Himalaya-Tibet orogen

The HTO is the result of ongoing collision between India and Asia, with the Indus suture zone defining the surface trace of the terminal collision (FIG. 3). The deforming region is bound to the south by the rigid Indian Craton and to the north by the rigid Tarim block, both of which underthrust the HTO. In the south, the orogen comprises the east–west trending Himalaya mountain range, which spans 2,500 km and is underlain by the thickest crust on Earth (up to 80 km)[12]. The orogen extends >1,000 km to the north in the form of the Tibetan plateau, which has an average altitude >5 km and is underlain by the thickest continental lithospheric root on Earth (up to 270 km)[18]. The laterally extensive central plateau is thought to have been at similar-to-modern elevations for at least 35 Myr (REF.[19]). The HTO itself is part of the greater Alpine-Himalayan belt, which extends for more than 7,000 km from the western Mediterranean to eastern China. The Alpine-Himalayan belt formed from the progressive and ongoing closure (since the Palaeozoic) of the Tethys Ocean and its modern remnants.

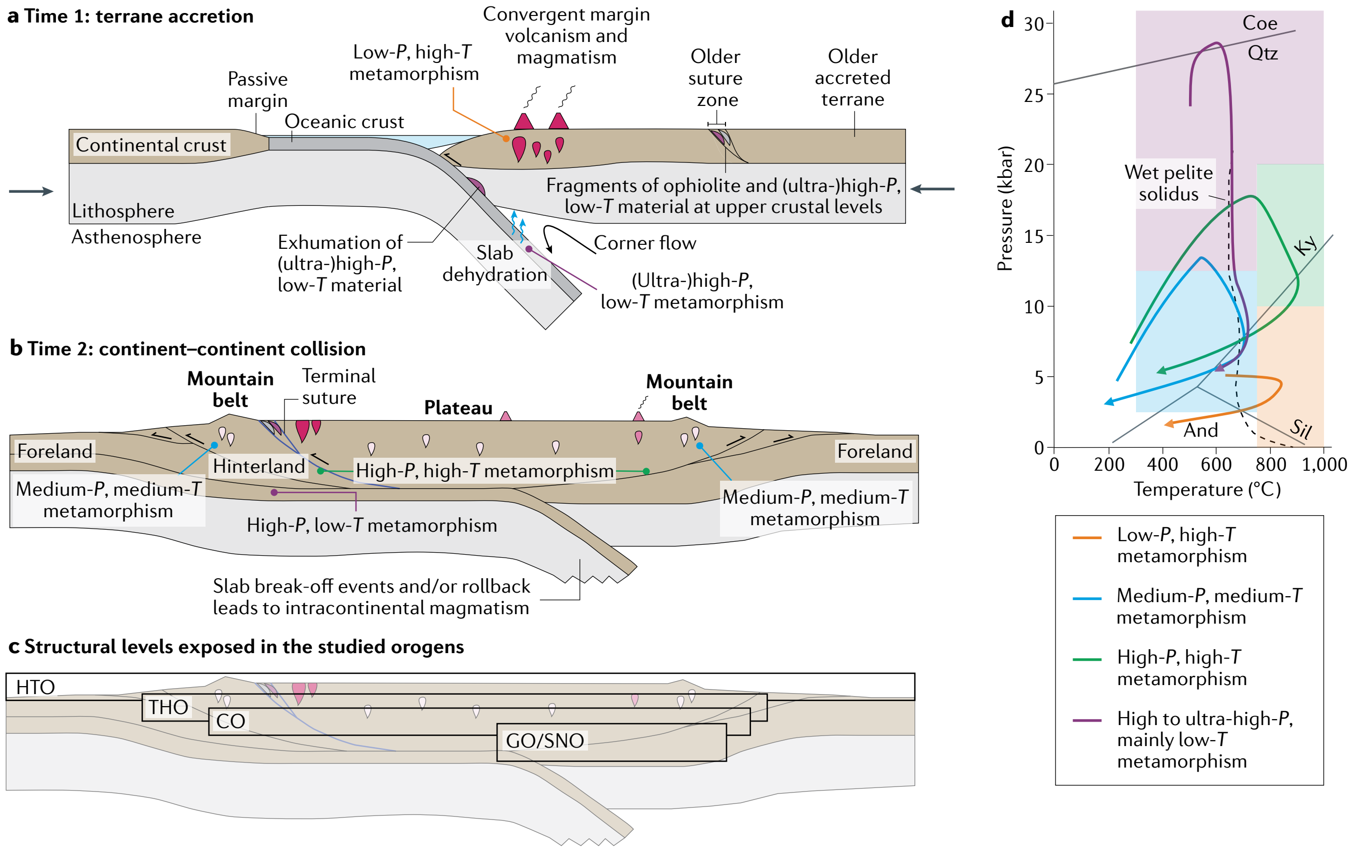

Fig. 1 | **The spatiotemporal development of metamorphic and magmatic rocks during collisional orogenesis.** The cross sections show typical processes that may occur during the evolution of a continent–continent collision. **a** | At time 1, a volcanic arc is present above a subducting oceanic plate in the continental upper plate, with the continental crust undergoing high-temperature (*T*), low-pressure (*P*) metamorphism, due to the elevated heat flow from widespread convergent margin magmatism. Continued convergence and subduction of the oceanic crust will eventually lead to collision with the leading edge of the trailing continent (the passive margin). **b** | At time 2, continent–continent collision has occurred, with the boundary between the collisional upper and lower plates marked by a suture zone. Metamorphic conditions typically increase in grade from medium-*T*, medium-*P* to high-*P*, high-*T* within the mountain belts and plateau, causing partial melting and the formation of leucogranites. **c** | After collision ceases, exhumation by faulting and erosion occurs, exposing deep crustal sections of the orogen. The schematic diagram highlights the average exposed structural level of the orogens reviewed in this paper: Caledonian orogen (CO), Grenville orogen (GO), Himalaya-Tibet orogen (HTO), Sveconorwegian orogen (SNO) and Trans-Hudson orogen (THO). **d** | Schematic *P*–*T* paths corresponding to the range of metamorphic conditions rocks might experience during orogenesis. The cross sections show where these *P*–*T* conditions are typically attained, but the precise thermal evolution of an orogen will vary depending on factors such as crustal thickness attained, convergence rate and radiogenic heat production. The quartz–coesite transition defines the boundary between high-*P* and ultra-high-*P* conditions. Aluminosilicate phase relations and the wet solidus for a pelite (mudstone) are shown for reference. And, andalusite; Coe, coesite; Ky, kyanite; Sil, sillimanite; Qtz, quartz.

Petrochronology
Determining the age of minerals within a petrographic context, such that the age(s) can be linked to stage(s) of metamorphism.

Orogen
Refers to a mountain belt formed by plate convergence. The term orogeny is derived from the ancient Greek words ‘oros’ (mountain) and ‘genesis’ (origin or formation).

Terrane
A fault-bound crustal block distinguished from adjacent domains by distinct geological characteristics, including age, lithology, stratigraphy and geological history.

The timing of the India–Asia collision is contentious, with a non-exhaustive list of estimates including 61 Ma (the timing of a stratigraphically defined India to Asia provenance reversal on the Indian passive margin)[20], 54 Ma (when zircons of Asian affinity were deposited on the Indian plate)[21], 51 Ma (the youngest marine sedimentary strata in the suture zone)[22], >47 Ma (the maximum age constraint on the post-collisional molasse)[23] or multistage from 50–40 Ma (based on the changing source region of arc magmatism as inferred from isotopic analyses)[24]. As estimates vary depending on the proxy used, part of the disagreement could be based on differences in definitions. The estimates also vary based on geographic location, suggesting that the age spread might be partly due to the diachroneity of collision[24]. Consequently, as a datum for FIG. 2. the view that collision occurred at 50 ± 10 Ma is adopted, and a minimum uncertainty of 10 Myr is ascribed to the timing of terminal collision for all orogens in this Review, unless indicated otherwise. This time interval is an order of magnitude less than the total duration analysed for each orogen (±100 Myr) (FIG. 2).

Total India–Asia convergence after collision is estimated at ~2,400–3,200 km, with approximately 450–900 km of the shortening thought to have been accommodated across the Himalaya and the remainder diffusely distributed across the Tibetan plateau and bordering ranges[25]. This latter far-field deformation, which includes uplift of mountain ranges to the north and to the west of Tibet (including the Pamir, Tien Shan and Mongolian Altai), provides insight into the scale of active tectonics potentially associated with orogens of this size.

Asian units

The southern margin of Asia experienced successive accretion events leading up to terminal collision with India, as a series of terranes — the Kunlun,

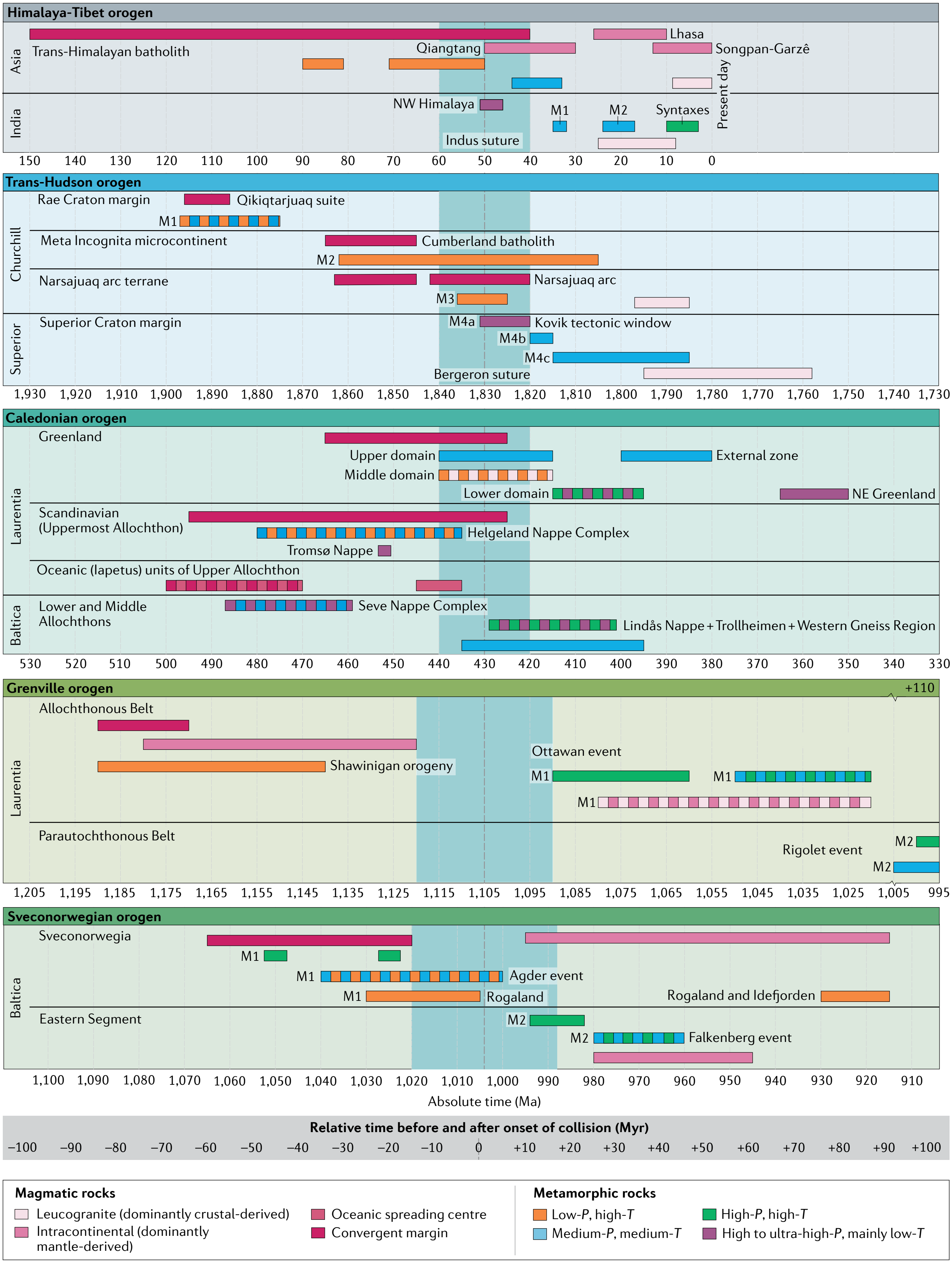
Himalaya-Tibet orogen
Asia
Trans-Himalayan batholith
Qiangtang
Lhasa
Songpan-Garzê
Present day
India
NW Himalaya
M1
M2
Syntaxes
Indus suture
150 140 130 120 110 100 90 80 70 60 50 40 30 20 10 0
Trans-Hudson orogen
Churchill
Rae Craton margin
Qikiqtarjuaq suite
M1
Meta Incognita microcontinent
Cumberland batholith
M2
Narsajuaq arc terrane
Narsajuaq arc
M3
Superior
Superior Craton margin
M4a
Kovik tectonic window
M4b
M4c
Bergeron suture
1,930 1,920 1,910 1,900 1,890 1,880 1,870 1,860 1,850 1,840 1,830 1,820 1,810 1,800 1,790 1,780 1,770 1,760 1,750 1,740 1,730
Caledonian orogen
Laurentia
Greenland
Upper domain
External zone
Middle domain
Lower domain
NE Greenland
Scandinavian (Uppermost Allochthon)
Helgeland Nappe Complex
Tromsø Nappe
Oceanic (Iapetus) units of Upper Allochthon
Baltica
Lower and Middle Allochthons
Seve Nappe Complex
Lindås Nappe + Trollheimen + Western Gneiss Region
530 520 510 500 490 480 470 460 450 440 430 420 410 400 390 380 370 360 350 340 330
Grenville orogen
+110
Laurentia
Allochthonous Belt
Ottawan event
Shawinigan orogeny
M1
M1
M1
Parautochthonous Belt
Rigolet event
M2
M2
1,205 1,195 1,185 1,175 1,165 1,155 1,145 1,135 1,125 1,115 1,105 1,095 1,085 1,075 1,065 1,055 1,045 1,035 1,025 1,005 995
Sveconorwegian orogen
Baltica
Sveconorwegia
M1
M1
Agder event
M1
Rogaland
Rogaland and Idefjorden
Eastern Segment
M2
M2
Falkenberg event
1,100 1,090 1,080 1,070 1,060 1,050 1,040 1,030 1,020 1,010 1,000 990 980 970 960 950 940 930 920 910
Absolute time (Ma)
Relative time before and after onset of collision (Myr)
−100 −90 −80 −70 −60 −50 −40 −30 −20 −10 0 +10 +20 +30 +40 +50 +60 +70 +80 +90 +100
Magmatic rocks
Leucogranite (dominantly crustal-derived)
Intracontinental (dominantly mantle-derived)
Oceanic spreading centre
Convergent margin
Metamorphic rocks
Low-P, high-T
Medium-P, medium-T
High-P, high-T
High to ultra-high-P, mainly low-T

◀ Fig. 2 | **The metamorphic and magmatic rock record for five major collisional orogens.** The orogenic 'barcode' outlines the key metamorphic and magmatic events that occurred within ±100 Myr before and after the onset of collision for each studied orogen. The orogens are ordered by exposed structural level (FIG. 1c), with the mean estimate for the onset of collision (dashed grey line) used as a common datum. Uncertainty on the timing of collision is represented by the central blue shading. All constraints are referenced in the text. M1, metamorphic event 1 (and so on); *P*, pressure; *T*, temperature. The *P*–*T* regions relevant to each metamorphic colour shading are shown in FIGURE 1. BOX 1 provides background detail to some of the concepts featured in this figure.

Songpan-Garzê, Qiangtang and composite Lhasa terranes — were progressively docked from the south beginning in the Permian[14,26,27] (FIG. 3). The accretion events occurred along a series of north-dipping sutures containing ophiolite fragments and relict high-pressure (HP) metamorphic assemblages[28,29], and were associated with the closure of the intervening Palaeotethys and Mesotethys oceans. Prior to the terminal collision with India, the southern edge of continental Asia experienced long-lived subduction of the Neotethys Ocean, with extensive calc-alkaline plutonism (the Trans-Himalayan batholith) and associated volcanism occurring from the early Jurassic to Eocene[23,30], yielding a thick and hot crust that underwent mid-crustal sillimanite-grade metamorphism and anatexis between ~90–81 Ma (REF.[27]) and ~71–50 Ma (REF.[31]).

Following collision, arc magmatism in southern Tibet waned, as cold Indian lithosphere underthrust Tibet[32]. Where deeper structural levels are exposed, anatexis in the kyanite stability field is recorded at ~44–33 Ma, resulting from crustal thickening following collision[31]. Abundant post-collisional magmatism, which is mostly potassic in nature and attributed to small-volume partial melting of enriched subcontinental lithospheric mantle, has been documented across the Tibetan plateau, including at ~50–30 Ma in the Qiangtang terrane, 26–10 Ma in the composite Lhasa terrane and ~13 Ma to the present in the Songpan-Garzê terrane[32]. These data have been used to infer the tectonic evolution of the Tibetan plateau, with further constraints provided by studies of entrained xenoliths that record Neogene granulite-facies conditions in the mid-lower crust[33,34]. The petrological observations have subsequently informed thermal models of the Tibetan plateau, which indicate that mid-crustal anatexis is viable in the present day[35,36], a conclusion supported by mid-crustal seismic velocity anomalies[37] and the observation of crust-derived <10-Ma silicic melts, where deeper structural levels of the plateau are exposed[38–40]. Less attention has focussed on the northern margin of the Tibetan plateau, but it is known that shortening is active (although at lower rates than the Himalaya)[41], accommodated by underthrusting of the Tarim block[42].

Molasse
A sedimentary rock type that comprises terrestrial or shallow marine strata deposited in front of rising mountain chains, typically including conglomerates.

Anatexis
Partial melting of rocks due to changes in the ambient pressure and/or temperature beyond the conditions at which rocks start to melt (the solidus).

Barrovian-type
A style of regional metamorphism named after British geologist George Barrow (1853–1932) and relating to pressure–temperature conditions typical of mid-crustal metamorphism during orogenesis.

Indian units

Prior to collision, the Indian plate comprised a stable craton overlain by a sequence of Proterozoic to Eocene sedimentary rocks along its northern passive margin and in long-lived intra-cratonic basins[43]. Following collision, rheological stratification of the Indian plate yielded divergent crustal responses: strong Indian lower crust and lithosphere underthrust Tibet for at least 500 km beyond the present-day range front[13,35] and contributed to the development of the plateau, whereas the upper crust underwent thrust imbrication to form the Himalaya[15,25]. Deformation in the latter was characterized by south-verging thrusts propagating down section from ~50–40 Ma along the Indus suture to present-day thrusting in the foothills of the Himalaya along the Main Frontal Thrust (FIG. 3), which breaks in magnitude 7–8 earthquakes[4].

The structure of the Himalaya exhibits notable continuity along-strike, with three major ductile-brittle shear zones (in addition to the Main Frontal Thrust) recognizable along the length of the mountain belt (FIG. 3): the South Tibetan Detachment, the Main Central Thrust and the Main Boundary Thrust. These structures are underlain by the Main Himalayan Thrust décollement at depth, collectively dividing the Himalaya into four lithotectonic units[15]. First, and structurally highest, is the Tethyan Himalayan Sequence, which is a folded sequence of (meta)sedimentary rocks that includes ophiolite fragments[44]. Second is the Greater Himalayan Sequence, which forms the backbone of the mountain belt and features the highest metamorphic grades[45]. Third is the Lesser Himalayan Sequence, a low-grade metasedimentary fold and thrust belt[46]. Finally, the structurally lowest unit is the Sub-Himalayan Zone, which comprises Miocene to Pleistocene sedimentary units derived from erosion of the active mountain belt[47].

Metamorphism in the Himalaya is commonly described in four phases[16,45,48], although these can equally be considered as petrological reference points in a continuously evolving thermal regime, with cumulative evidence of metamorphism from ~50 to <10 Ma (REFS[48,49]) at different locations along the belt. The earliest metamorphism is recorded by coesite-bearing eclogite[50] in the Kaghan area of northern Pakistan and the Tso Morari region of north-west India, which have yielded peak pressures of 27–29 kbar at ~51–46 Ma. Owing to this timing and the location of the eclogites along the northern exposed margin of the Indian plate (FIG. 3), the ultra-high-pressure (UHP) metamorphism has been attributed to deep continental underthrusting during the early stages of collision.

The second phase of metamorphism (commonly referred to as M1) occurs regionally in the Greater Himalayan Sequence, is of Barrovian-type and features kyanite-bearing assemblages that have yielded peak *P*–*T* conditions of 550–680 °C and 10–12 kbar at ~35–32 Ma (REF.[16]). The third phase of metamorphism (commonly referred to as M2) features peak sillimanite-bearing assemblages of 650–700 °C and 3.7–4.5 kbar at ~24–17 Ma (REF.[16]). These M2 assemblages are coeval with widespread partial melting by muscovite-dehydration melt reactions, which produced the kilometre-scale ~25–15 Ma Himalayan leucogranite bodies in the Greater Himalayan Sequence[51], with younger leucogranite bodies (to ~8 Ma) recorded in the eastern Himalaya[52]. Inversion of the Barrovian sequence at the base of the Greater Himalayan Sequence occurred progressively as material was accreted in the Main Central Thrust zone during the Miocene[53,54]. The fourth phase is recorded in the cores of the Nanga Parbat and Namche Barwa syntaxes[55] (FIG. 3),

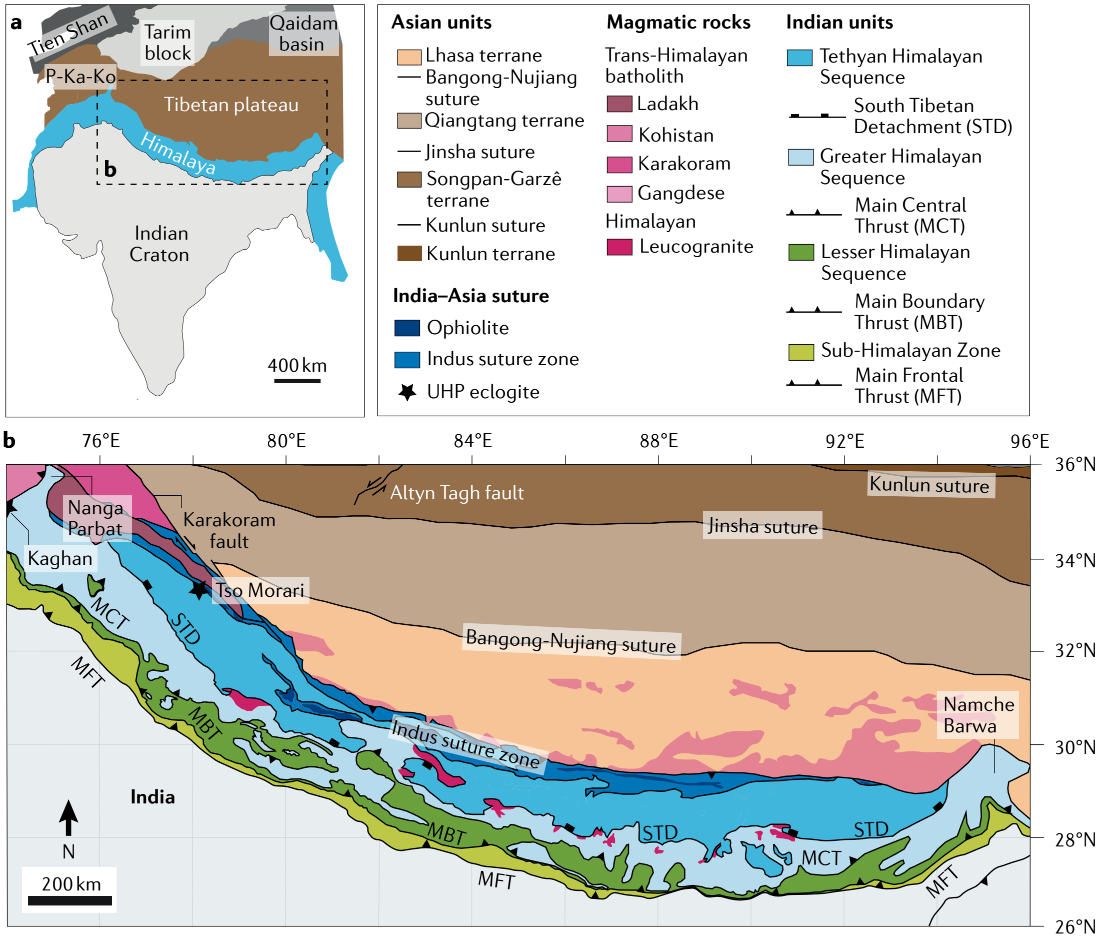

Fig. 3 | **Geological map of the Himalaya-Tibet orogen.** The Himalaya-Tibet orogen (HTO) is still actively deforming and is the product of continued India–Asia convergence. The timing of the onset of collision is contentious, with most estimates being in the range ~40–60 Ma. **a** | Overview of the HTO and bounding crustal blocks. **b** | Geological map of the HTO showing the key tectono-metamorphic and magmatic domains of the Himalaya (shades of blue–green) and the Tibetan plateau (shades of orange–brown), and the pre-collisional magmatic arc (shades of pink). The major orogenic faults and structures that accommodated shortening within the orogeny are also shown. The Bangong-Nujiang, Jinsha and Kunlun suture zones correspond to pre-collisional accretionary events, prior to terminal collision along the Indus suture zone. P-Ka-Ko, Pamir-Karakoram-Kohistan; UHP, ultra-high pressure. Panels **a** and **b** adapted from REF.[227], CC BY 4.0 (https://creativecommons.org/licenses/by/4.0/).

where focussed exhumation has provided a window into deeper structural levels of the orogen and revealed granulite-facies conditions of 10–14 kbar and 700–900 °C at 10–3 Ma (REF.[56]).

Despite the metamorphic conditions of the Himalaya being well documented, the characteristics and evolution of the deformation remain debated, with alternative suggestions emphasizing the importance of ‘channel flow’[57,58], critical taper[59], simple shear above the rigid underthrusting part of the Indian plate[60] or mid-crustal duplexing[61], some aspects of which are not mutually exclusive. Temporal and spatial variations along the orogen have been identified, suggesting that exhumation of the metamorphic core could have been a complex and heterogeneous process[16,44,62]. Advances in structural analysis[63] and the increasing synthesis of petrological and geodynamic modelling approaches[64] offer promising avenues for future research to constrain the evolution of the Himalayan orogenic core. Although abundant evidence of deformation has been recorded in lower-grade components of the Himalaya[47], the equivalent rocks are rarely preserved in older orogens due to erosion, so they are not discussed further in this Review.

The Caledonian orogen

The CO extends from northern Greenland and Scandinavia southwards through the British Isles (FIG. 4a) and connects with the Appalachian Mountains in eastern North America. The CO forms a chain of mountains 7,500 km long that represents an early stage in the formation of Pangaea[65,66]. The CO resulted from the Ordovician–Silurian closure of the Iapetus Ocean, due to convergence between Laurentia and Baltica (the latter coupled to Avalonia). The protracted convergence involved accretion of oceanic terranes, with the terminal continental collision commencing at ~430 Ma (REFS[65,67,68]).

For this Review, it is appropriate to focus on the ~2,000-km-long Greenland–Scandinavia segment of the CO (which only involves Laurentia and Baltica),

Nappes
Large, sheet-like bodies of rock that have been moved some kilometres above a thrust fault from its original position (often synonymous with 'allochthon').

as this segment has been compared in terms of scale with the HTO[69,70]. This comparison is based on similar estimated crustal thicknesses of 70–80 km (REF.[69]) and estimated across-strike widths of ~1,000 km, before the orogen was divided by the North Atlantic Ocean, which opened during the Mesozoic and Cenozoic. The CO forms a bivergent orogenic wedge in this segment, with west-vergent nappes in Greenland and (mainly) east-vergent nappes in Scandinavia. The bivergent symmetry is thought to have resulted from both the colliding plates being dominated by cold and rigid, old (Archaean–Palaeoproterozoic) continental crust[70], analogous to India and the Tarim block. The Greenlandic nappes only expose Laurentian assemblages, whereas the Scandinavian nappes incorporate Laurentia-derived crustal units, Iapetan ophiolites and island arcs, and Baltican basement and cover units[65,67,68,71,72]. The abundance of calc-alkaline plutonism in units derived from Laurentia and the Iapetus Ocean indicates that the pre-collisional subduction zone dipped beneath Laurentia.

Laurentian and Iapetan units

Greenland. Prior to collision, the Greenland segment of the Caledonides formed a passive margin on the edge of Laurentia and comprised Archaean to Mesoproterozoic

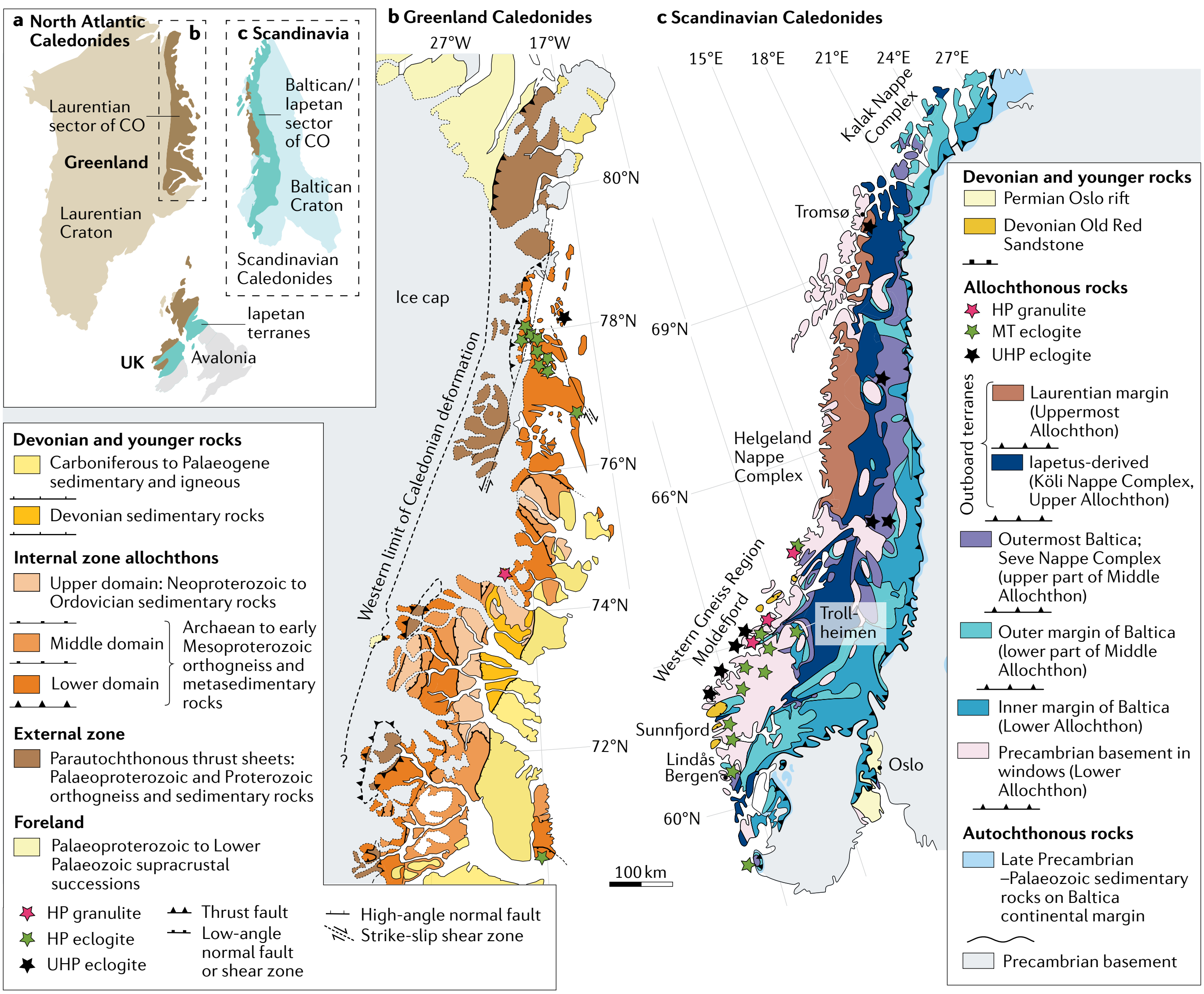

Fig. 4 | **Geological maps of the Caledonian orogen.** The collision between Laurentia, Baltica and Avalonia occurred at ~430 Ma to form the Caledonian orogen (CO), during the early stages of the assembly of the supercontinent Pangaea. The ~mid to lower crustal levels of this orogen are currently exposed in Greenland, Scandinavia and the northern UK. **a** | Overview of the North Atlantic Caledonides. The different continental blocks are shown in their approximate relative positions at the end of the Caledonian orogeny, prior to the Cenozoic seafloor spreading that formed the present-day North Atlantic Ocean. **b** | Geological map of the CO exposed in Greenland. The major thrust nappes have a Laurentian affinity and dip mainly south-eastwards. **c** | Geological map of the CO exposed in Scandinavia. The major thrust nappes comprise units of Laurentian, Iapetan and Baltican affinities and dip mainly north-westwards. HP, high pressure; MT, medium temperature; UHP, ultra-high pressure. Panel **b** adapted with permission from REF.[228], Geological Survey of Denmark and Greenland. Panel **c** adapted with permission from REFS[229,230], © Geological Survey of Sweden and © Geologiska Föreningen, reprinted with permission of Informa UK Limited, trading as Taylor & Francis Group, www.tandfonline.com on behalf of Geologiska Föreningen.

Allochthonous
A package of rocks that were originally formed or deposited a substantial distance from their current location, and were transported by tectonic processes.

Anchizone
The transitional zone between diagenesis and metamorphism; this is normally characterized by low temperatures (100–200 °C) and pressures (1–2 kbar).

Isothermal decompression
Exhumation of a rock mass at approximately constant temperature, indicating exhumation rates more rapid than rates of heat transfer.

Parautochthonous
A package of rocks that have been displaced a relatively small distance from their original place of formation and can still be correlated with the footwall lithostratigraphic units.

Buchan
A style of regional metamorphism characterized by the presence of andalusite in intermediate-grade pelitic assemblages, indicating lower pressure metamorphic conditions than Barrovian.

rocks overlain unconformably by Neoproterozoic to Ordovician sedimentary rocks[73]. Following collision, two tectonic divisions are recognized: the internal and external zones (FIG. 4b).

The internal zone corresponds to the outermost part of the passive margin. This region was thrusted and folded during early stages of the orogeny to result in substantial crustal thickening and high-pressure metamorphism[74–76]. Extensional collapse and exhumation of deeply buried crustal segments[74–77] was followed by thrusting of the internal zone westwards over the external zone.

The external zone corresponds to the inner part of the passive margin and includes Cambrian to Silurian sedimentary rocks that can be correlated with the foreland of the orogen[78] (FIG. 4b). In broad terms, deformation and metamorphism propagated westwards, although there is overlap in the timing of exhumation in the internal zone and thrusting in the external zone[79,80]. Pre-collisional to syn-collisional subduction-related magmatism, lasting from 465 to 425 Ma (REF.[81]), is recognized only in the southernmost part of the orogen (south of 71°N).

Low-angle normal faults and shear zones divide the internal zone into upper, middle and lower allochthonous domains[74,75]. Metamorphic grade increases downwards, with notable jumps across the faults and shear zones. This structure is characteristic of the high-grade internal parts of orogenic belts, where deeply buried rocks have been exhumed during extensional faulting. The upper domain mainly records relatively low-grade metamorphism from anchizone to greenschist facies, consistent with upper crustal conditions (depths <15 km)[75]. In contrast, the underlying middle domain underwent melting to form abundant migmatites and leucogranites. Melting occurred at <10 kbar and temperatures of up to 850 °C, followed by near-isothermal decompression[75,82]. The rapid reduction in pressure corresponds to the exhumation of these rocks as they were juxtaposed by extensional faulting against the upper domain. Upper and middle domain metamorphism and melting are dated at ~440–415 Ma (REFS[82,83]). Contraction continued at deeper crustal levels, forming eclogite-facies and granulite-facies metamorphic assemblages in the lower domain (pink and green stars, FIG. 4b) at ~415–395 Ma (REFS[75,76]). Peak metamorphism occurred at pressures of 15–23 kbar and was again followed by isothermal decompression as these deeply buried rocks were exhumed and juxtaposed against the middle domain[74–76].

The internal zone was largely assembled tectonically by ~400–390 Ma and then thrust westwards onto the external zone. The foreland-propagating thrust and fold belt that developed within the parautochthonous rocks of the external zone is characterized by inverted Barrovian metamorphism, which decreases westwards from amphibolite facies to anchizone and, although poorly constrained, probably occurred at ~400–380 Ma (REF.[75]). West-directed thrusting and folding may have overlapped the final stages of extensional faulting in the overlying internal zone, as well as Middle Devonian sedimentation in supra-detachment basins (FIG. 4b). Marginal thrusting and late-orogenic strike-slip displacements along shear zones (FIG. 4b) continued through the Devonian[84]. Localized UHP metamorphism at 365–350 Ma recorded in the coastal region of Northeast Greenland (black star, FIG. 4b) has been attributed to late intracontinental underthrusting, potentially analogous to underthrusting of the Tarim block on the north side of the HTO[85].

Scandinavia. The Scandinavian Caledonides comprise a stack of thrust nappes, which are subdivided into a series of allochthons (Uppermost, Upper, Middle and Lower)[65,68,71] (FIG. 4c). The allochthons were translated south-eastwards onto and across the continental margin of Baltica; those at the top (Uppermost and Upper) were derived from Laurentia and the Iapetus Ocean and largely preserve pre-collisional metamorphic imprints, whereas those at the bottom (Middle and Lower) were predominantly sourced from Baltica.

The Uppermost Allochthon (FIG. 4c) is dominated by metasedimentary rocks intruded by Ordovician ~495–440 Ma granitoid plutons during protracted pre-collisional subduction along the active margin of Laurentia[86–89]. Nappes within this allochthon preserve variable metamorphism associated with this setting. In the Helgeland Nappe Complex[87], Barrovian to Buchan metamorphism and associated crustal anatexis occurred at ~480–435 Ma (REFS[87,88,90]). In the Tromsø nappe, UHP metamorphism peaked at ~34 kbar and 750 °C at ~452 Ma (REFS[91–93]), followed by exhumation and decompression melting at ~449 Ma. During the onset of continental collision, accretionary magmatism evolved to bimodal mafic and felsic at 440–425 Ma (REF.[89]).

Iapetan rocks in the underlying Upper Allochthon (FIG. 4c), which includes the Köli Nappe Complex as its largest entity (FIG. 4c), include Late Cambrian to Ordovician ophiolite and island-arc complexes (~500–470 Ma), and ~445–435 Ma ophiolite formed immediately prior to collision[94–96]. The Upper Allochthon was mostly metamorphosed under greenschist-facies or amphibolite-facies conditions, distinctly lower grade than the immediately underlying Baltica-derived nappes (Seve Nappe Complex, below).

Baltican units

The lower structural levels of the Scandinavian Caledonides (Middle and Lower Allochthons) (FIG. 4c) comprise multiple nappes derived mainly from the passive margin of the Baltica plate. The upper part of the Middle Allochthon includes the Seve Nappe Complex and upper Kalak nappes (FIG. 4c). The Seve Nappe Complex features high-grade metamorphic rocks, among them mafic meta-igneous rocks linked to the opening of Iapetus at the continent–ocean transition zone at 608 ± 1 Ma (REFS[97,98]), aluminous paragneiss and distal units, including mantle-derived rocks (such as garnet peridotite)[99–103]. Generally, the provenance of the outermost units is considered to be Baltican, although this affiliation is debated[72,104]. Pre-collisional, subduction-related, UHP metamorphism of parts of these complexes occurred between ~487 and 459 Ma (REFS[105–107]), with peak P–T estimates ranging from ~30 kbar and 700 °C to ~40 kbar and 850 °C (REFS[108,109]).

Nappes structurally below, in the lower–central levels of the Middle Allochthon and the Lower Allochthon, include both metasedimentary rocks and Precambrian

In-sequence
When fault age progressively decreases in the direction of transport.

basement rocks that experienced syn-collisional to post-collisional Barrovian metamorphism at ~435–395 Ma (REFS[110,111]). Syn-collisional to post-collisional eclogite-facies metamorphism is observed in some units, including ~429 Ma, ~22 kbar and 680 °C in the Lindås Nappe[112–114]; ~425 Ma in Trollheimen[115]; and ~415–401 Ma (REF.[116]) in the lowermost exposed tectonic level, the Western Gneiss Region (part of the Lower Allochthon). Collectively, these geochronological data document a west-to-east temporal progression of HP metamorphism, consistent with deep and in-sequence underthrusting of Baltica beneath Laurentia.

The Western Gneiss Region is one of the largest regions of exposed HP metamorphic rocks on Earth (~50,000 km^2)[117,118]. Studies of this region have been highly influential in developing understanding of deep crustal metamorphic processes, including the role of metastability[119,120]. The Western Gneiss Region is dominated by Baltica basement, featuring both in situ metamorphosed gabbro-to-eclogite[121] and tectonically emplaced garnet peridotite fragments from the Laurentian mantle[122]. The Western Gneiss Region experienced HP to UHP metamorphic conditions, ranging from 500 °C and 16 kbar in the south-east to >800 °C and 32 kbar in the north-west, followed by near-isothermal exhumation at amphibolite-facies to granulite-facies conditions[117,118,123].

The large-scale in-sequence thrust architecture of the Scandinavian Caledonides has been modified by other syn-collisional and post-collisional structures. For example, a late-stage thrust has been documented locally at the top of the Seve Nappe Complex[124]. Regional extension, vertical thinning and exhumation of the Scandinavian Caledonides, beginning at ~400 Ma, resulted in east-to-west backsliding of nappes along décollements[125], the formation of extensional basins and crustal partial melting[126]. Despite these late-orogenic modifications, the Scandinavian Caledonides represent a remarkably complete vertical section through a collisional orogen, from fragments of the upper continental plate, down through oceanic and passive margin units and into the deeply buried basement of the lower continental plate.

Grenville and Sveconorwegian orogens

The Grenville and Sveconorwegian orogens (FIG. 5) are fragments of a much larger orogenic belt formed during assembly of the supercontinent Rodinia at ~1.1 Ga (REF.[127]). Both orogens are inferred to have featured double-thickness crust (70–80 km) and widespread high-temperature metamorphism at ~1,100–900 Ma (REFS[128–131]). Both orogens have been deeply exhumed to expose their lower crustal roots. The Grenville orogen (GO) is exposed in a 2,000 × 500 km^2 region on the south-eastern margin of Laurentia (eastern Canada) and the Sveconorwegian orogen (SNO) forms a 600 × 600 km^2 region on the western margin of Baltica (southern Norway and Sweden). The GO is frequently described as a 'large hot orogen'[58,128,132–134], owing to the preservation of a range of crustal depths juxtaposed during extensional collapse of a wide orogenic plateau. The SNO is the Baltican counterpart of the GO[129,130]. Several models have been proposed to explain the configurations of Laurentia and Baltica within Rodinia[127,135–138], and, although constraints are improving, a robust consensus remains out of reach.

In both the GO and the SNO, only parts of the orogen and one of the bounding crustal blocks are exposed because of subsequent rifting. In the GO, all exposed crust is of Laurentian affinity. The suture between Laurentia and Amazonia (inferred to be the other colliding plate[135]) may be preserved in allochthonous inliers of the southern Appalachians[128]. For the SNO, different reconstructions have been proposed, involving variable plate configurations and candidates for suture zones, with end-member suggestions being that the SNO represents a prolonged Cordilleran-type orogen with a long-lived active margin or that it is a collisional orogen[129]. Herein, the SNO is considered to have formed by collisional orogenesis, with the Mylonite Zone (FIG. 5c) corresponding to the deep-seated (30–40-km-deep) trace of a suture zone that separated Palaeoproterozoic Baltica (Eastern Segment) from a composite allochthonous terrane (Sveconorwegia)[130,139].

The timing of collision is difficult to constrain for both orogens. For the GO, the onset of collision is bracketed between ~1,120 Ma, the end of pre-collisional magmatism, and ~1,090 Ma, the initiation of high-grade metamorphism in the mid-crust[128]. For the SNO, the onset of collision is inferred between ~1,020 Ma, the end of calc-alkaline magmatism in Sveconorwegia[129], and 988 ± 6 Ma, the age of high-temperature eclogite-facies metamorphism in the Eastern Segment[130].

The Grenville orogen

The GO was preceded by ≥600 Myr of accretionary tectonics that record progressive closure of a large ocean basin[140]. A wide ductile shear zone (the Allochthon Boundary) divides the GO into two main lithotectonic elements (FIG. 5b): the Parautochthonous Belt and the Allochthonous Belt[128,141]. The Parautochthonous Belt consists of Archaean and Palaeoproterozoic rocks derived from Laurentia. The Allochthonous Belt consists of several entities, including: imbricated Mesoproterozoic (1,600–1,350 Ma) arc and backarc terranes, formed on and proximal to the Laurentian margin, with subordinate accreted island-arc terranes; the Composite Arc–Frontenac-Adirondack belt, which consists of a Late Mesoproterozoic (≤1,300 Ma) arc and backarc terranes, also formed on and proximal to the Laurentian margin, together with remnants of oceanic crust and arc magmatism from 1,190–1,170 Ma; and several large anorthosite–mangerite–charnockite–granite igneous complexes emplaced from 1,180–1,120 Ma (REF.[128]). The latter igneous complexes were derived from mantle and crustal sources and constitute a signal of limited extension predating collision at ~1.1 Ga.

Two main episodes of metamorphism are documented in the GO: M1, which is commonly referred to as the Ottawan event, at ~1,090–1,020 Ma, and M2, which is referred to as the Rigolet event, at 1,005–985 Ma. Much of the Allochthonous Belt consists of migmatitic, granulite-facies gneisses that yield peak (M1) P–T conditions of ~11 kbar and 850–950 °C at ~1,090–1,060 Ma (REFS[142,143]), and comparable P–T conditions and timing

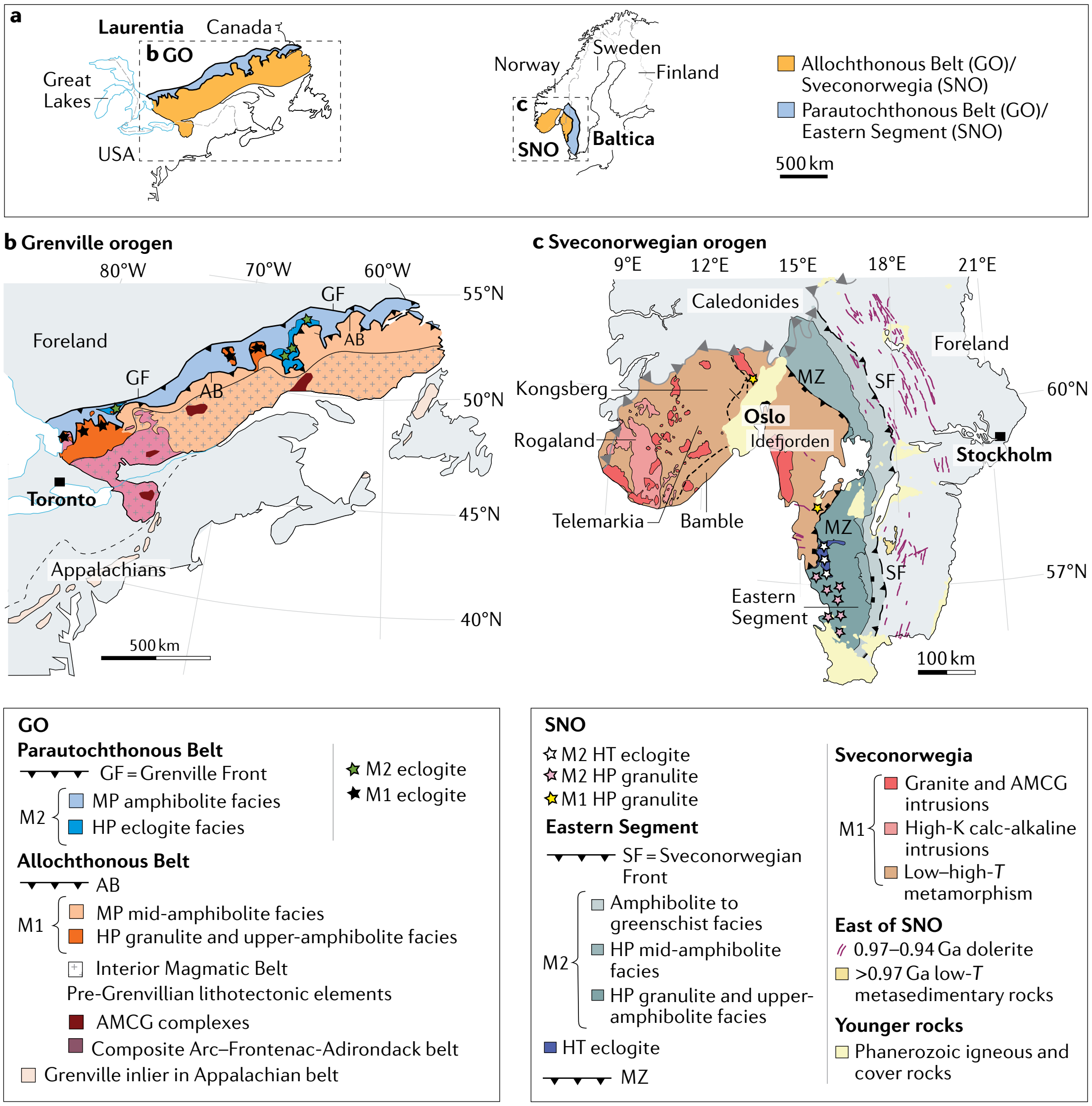

Fig. 5 | **Geological maps of the Grenville and Sveconorwegian orogens.** These orogens formed during the assembly of the supercontinent Rodinia at ~1 Ga, and their deeply exhumed roots are now exposed across Eastern Canada (Grenville orogen (GO)) and southern Norway and Sweden (Sveconorwegian orogen (SNO)). **a** | Overview of the main elements of the GO and the SNO. Although the GO and SNO were previously considered to be parts of a single orogenic belt developed on the margin of composite Mesoproterozoic Laurentia–Baltica[231], pre-Rodinian continuity between Laurentia and Baltica is now disputed and the GO and the SNO may have developed as proximal but separate orogens within Rodinia[135,137]. **b** | Overview map of the GO, which is composed of two main domains: the Parautochthonous Belt (blue shades) and the Allochthonous Belt (orange to brown shades), divided by a ductile shear zone (the Allochthon Boundary (AB))[128]. **c** | Overview map of the SNO, which is composed of two main domains: the Eastern Segment and Sveconorwegia, divided by a ductile shear zone (the Mylonite Zone (MZ)). The Sveconorwegian Front marks the eastern limit of Sveconorwegian ductile deformation. M1 (metamorphic event 1) and M2 (metamorphic event 2) occurred at overlapping times in the GO and the SNO. AMCG, anorthosite–mangerite–charnockite–granite; HP, high-pressure; HT, high temperature; MP, medium pressure; *T*, temperature. Panel **a** adapted with permission from REF.[129], Elsevier. Panel **c** adapted with permission from REFS[130,139], Elsevier and Wiley, © 2018 John Wiley & Sons Ltd.

have been reported from Grenvillian inliers derived from Amazonian crust in the central Appalachians[144]. The M1 event, thus, spanned the orogenic suture zone and the *P*–*T* conditions are interpreted to have occurred near the middle of double-thickness crust[128]. High-pressure eclogite-facies relics near the Allochthon Boundary were formed near the base of the thickened crust (peak *P* conditions ~17 kbar)[143,145] and underwent substantial heating during exhumation into the granulite-facies mid-crust. Subsequent extensional juxtaposition of domains with high-pressure, medium-pressure and low-pressure M1 assemblages is attributed to orogenic collapse after the M1 metamorphic peak between 1,050 and 1,020 Ma (REFS[146,147]). M1 metamorphism overprinted pre-Grenvillian, accretionary granulite-facies metamorphic rocks at many locations, including those formed in the ~1,190–1,140-Ma Shawinigan orogeny.

Grenvillian M2 metamorphism took place from 1,005–985 Ma (REF.[128]) and is best preserved in the Parautochthonous Belt. It was Barrovian-style and is associated with structures ranging from a crustal-scale shear zone[148] to an orogenic wedge, with an inverted metamorphic sequence that increases in grade structurally upwards from greenschist facies to uppermost amphibolite facies, and locally high-pressure granulite facies at 1,000–90 Ma (REFS[149–151]). These tectonic relationships suggest that M2 developed during southward underthrusting of Laurentian crust beneath the orogenic plateau, a setting analogous to that of the Tarim block in the HTO.

Magmatism during M1 and M2 occurred in the Interior Magmatic Belt, which overlaps the Allochthonous and Composite Arc–Frontenac-Adirondack belts[128,141], and is spatially distinct from the locus of Barrovian metamorphism in the Parautochthonous Belt at the orogen margin[152] (FIG. 5b). Magmatism during M1 from ~1,080–1,020 Ma was compositionally diverse, and included leucogranite, monzogranite, gabbro, small anorthosite–mangerite–charnockite–granite complexes and ultrapotassic intrusions. Collectively, this magmatism is indicative of crustal, lithospheric mantle and asthenospheric sources, with the latter interpreted to imply delamination or rollback of the overthickened orogenic lithosphere[153]. Magmatism during M2 from ~995–950 Ma exhibited similar diversity but was less voluminous.

The Sveconorwegian orogen

The SNO (FIG. 5a,c) consists of two main domains: the structurally lower Eastern Segment (Palaeoproterozoic in origin, with subordinate 1,400-Ma and 1,220-Ma intrusions) and the structurally higher Sveconorwegia (of dominantly Mesoproterozoic origin). The Sveconorwegia domain is further subdivided into four segments: Idefjorden, Bamble, Kongsberg and Telemarkia (which also includes Rogaland)[129,130,139,154]. The Mylonite Zone[155,156] is a gently west-dipping ductile shear zone that is several kilometres wide and separates the Eastern Segment from Sveconorwegia. The SNO features two main stages of metamorphism[129,130,139]. The early stage (M1) at 1,050–1,000 Ma is recorded in Sveconorwegia only and, because of its association with calc-alkaline magmatism, is inferred as pre-collisional to syn-collisional. The later stage (M2), at 988–960 Ma, caused regional high-pressure metamorphism (~40 km depth) of the Eastern Segment and is regarded as syn-collisional to post-collisional. These two phases of metamorphism overlap in time with the M1 and M2 phases of the GO[128,130]. The M2 phase developed during westward underthrusting of Baltican crust beneath Sveconorwegia, a setting that can be interpreted as an analogue of the Indian plate or the Tarim block underthrusting the Tibetan plateau[129,130,139].

Much of Sveconorwegia underwent mid-crustal metamorphism. However, Bamble, Kongsberg and parts of Telemarkia represent crustal domains that occupied upper crustal levels during the Sveconorwegian M1 phase and were later downfaulted[129]. Western Sveconorwegia (Telemarkia) was intruded by a 300-km-long belt of high-K calc-alkaline granite magmas between ~1,065 and 1,020 Ma, for which two competing tectonic interpretations have been proposed: syn-collisional crustal melting[129] versus convergent-margin magmatism[157] (the latter hypothesis is shown in FIG. 2). Regional metamorphism in Sveconorwegia (M1) was broadly coeval with the calc-alkaline magmatism. The M1 phase included mid-crustal upper-amphibolite metamorphism and migmatization at 1,040–1,000 Ma (the Agder event[129]) and ultrahigh-temperature metamorphism at ~1030–1005 Ma in Rogaland[158,159]. In addition, M1 high-pressure granulite-facies rocks are present locally in the lowermost eastern part of Sveconorwegia (Idefjorden), dated at ~1,050 and 1,025 Ma (REFS[160,161]) (FIG. 5c). These relationships suggest that Sveconorwegia represents a collapsed part of an orogenic plateau, and that its deepest levels are exposed along the contact with the Eastern Segment.

Post-collisional magmatism[129] (<995 Ma) in Sveconorwegia includes dominantly granite plutons with subordinate gabbro that intruded at 985–915 Ma and anorthosite–mangerite–charnockite–granite complexes at 937–915 Ma (REFS[129,162,163]). The latter are associated with ultrahigh-temperature contact metamorphism between ~930 and 915 Ma at low pressure (4–5 kbar)[158,159,163]. This magmatism was partly sourced from the mantle and persisted through the waning stages of orogenic collapse.

The parautochthonous Eastern Segment is in lithological continuity with Baltica, east of the Sveconorwegian Province[130,139,164]. From east to west, regional (M2) metamorphism and polyphase deformation at 980–960 Ma grades from epidote amphibolite to upper amphibolite and high-pressure granulite facies (the Falkenberg event)[130,139,165]. A large part of the Eastern Segment records M2 pressures of ~10 kbar. This regional M2 metamorphism was synchronous with the exhumation of an eclogite-bearing terrane[139,166], which records peak M2 conditions of 18–19 kbar and ~870 °C at 988 ± 6 Ma (REFS[130,167,168]), and is situated immediately beneath the tectonic contact with Sveconorwegia. The eclogite-facies metamorphism testifies to deep tectonic burial (~65 km) of the leading edge of the Eastern Segment beneath Sveconorwegia.

In the Eastern Segment, metamorphic recrystallization and migmatization were controlled by the ingress of hydrous fluid[139,169,170]. This recrystallization behaviour is similar to that of the 'dry' basement of the Scandinavian Caledonides[112,119,120] (see CO section) and shows that igneous continental crust commonly remains unreacted (metastable) in the absence of fluid. The Sveconorwegian Front (FIG. 5c) marks the eastern limit of deformation[171] at the present erosion level. However, upper levels of the orogen are interpreted to have extended ~200 km farther east[139,172]. Late to post-orogenic extension-related intrusions are restricted to 960–935-Ma granitic pegmatite dykes and 980–945-Ma dolerite dykes along and east of the Sveconorwegian Front[130,139,173].

The Trans-Hudson orogen

The ~1,830–1,758-Ma THO[174,175] comprises erosional remnants of a collisional mountain belt that extended ~4,600 km across North America (FIG. 6a) and constituted part of the Nuna supercontinent[174]. The THO formed due to collision of the Archaean Superior Craton with a collage of Archaean and Palaeoproterozoic crustal blocks (collectively known as the Churchill plate)

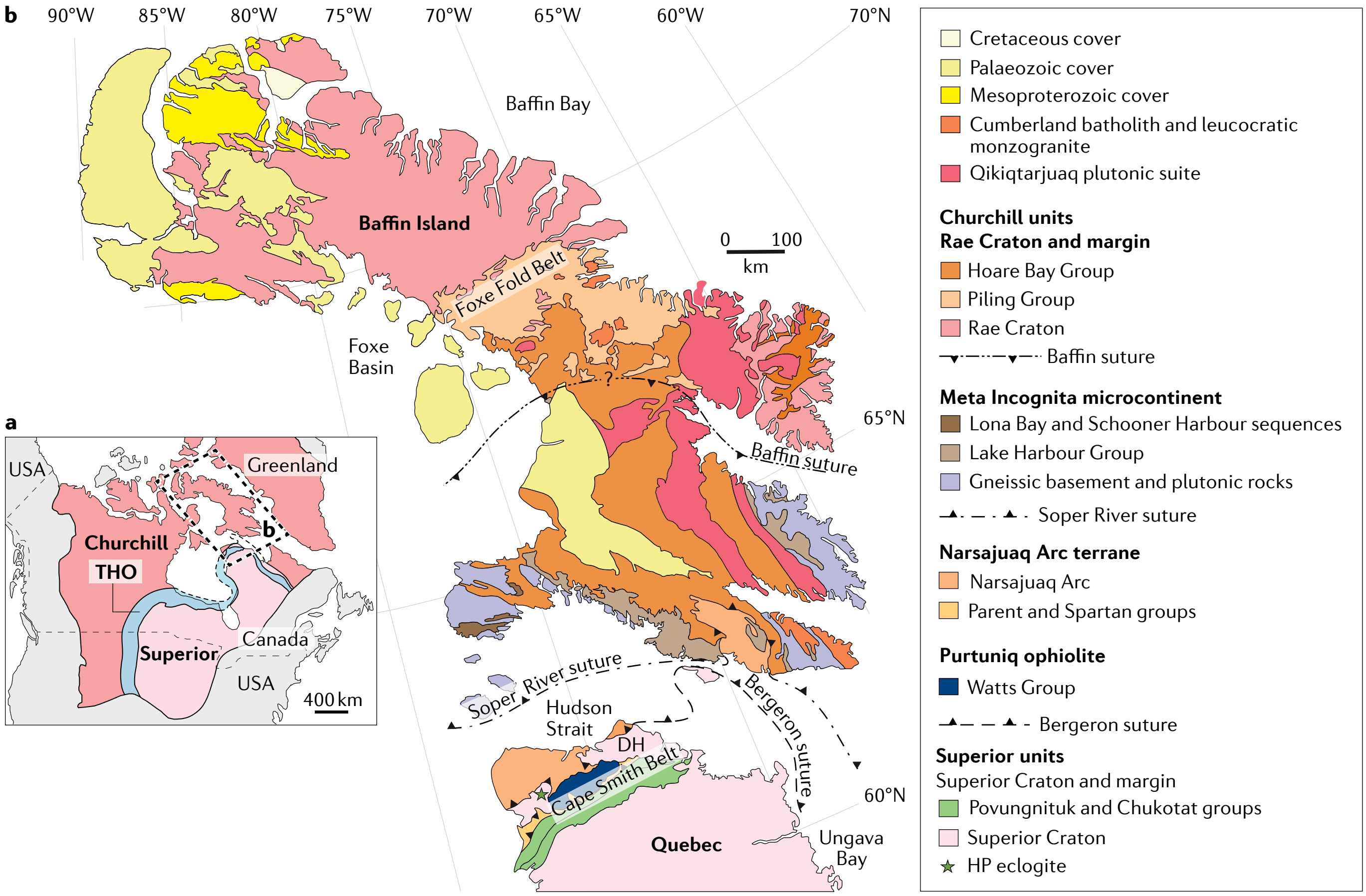

Fig. 6 | **Geological map of the Trans-Hudson orogen.** The Trans-Hudson orogen (THO) formed ~1,830–1,758 Ma during the assembly of the Nuna supercontinent and extended across North America. The upper to lower structural levels of the orogen are well exposed on Baffin Island and northern Quebec, Canada. **a** | Overview of the extent of the THO, the Churchill collisional upper plate and the Superior collisional lower plate across North America. **b** | The main map shows the key lithostratigraphic and magmatic units (coloured) and major orogenic structures that have accommodated shortening within the Arctic Canada segment of the THO. Key sutures include Baffin, Soper River and (terminal) Bergeron, which each correspond to individual accretionary and collisional events discussed in the text. Post-Palaeoproterozoic cover is shown in grey. DH, Douglas Harbour window; HP, high pressure. Panel **a** adapted from REF.[178], Springer Nature Limited. Panel **b** adapted with permission from REF.[183], © Her Majesty the Queen in Right of Canada, as represented by the Minister of Natural Resources, 2020. https://open.canada.ca/en/open-government-licence-canada. Panel **b** adapted with permission from REF.[189], © Her Majesty the Queen in Right of Canada, as represented by the Minister of Natural Resources, 2017. Panel **b** adapted with permission from REF.[232], Canada-Nunavut Geoscience Office.

at ~1,830 Ma (REFS[176–183]). The collision occurred following progressive closure of the Manikewan Ocean, during which intervening allochthonous terranes were accreted to the Churchill plate, which formed the upper plate at the onset of collision. Thermal and deformational effects associated with the collision are documented 800 km across-strike[177,184], and Moho depths were likely to have been 60–70 km when the orogen was active[185]. The THO is particularly well preserved in its north-eastern segment in Arctic Canada, the region described here, where the presence of a Palaeoproterozoic ophiolite sequence indicates that the upper structural levels of the orogen are exposed at the present erosion surface.

Thin-skinned
When deformation only involves cover (and not basement) units; when both elements are involved, deformation is referred to as thick-skinned.

Churchill units

In the ~80 Myr prior to terminal collision with the Superior Craton, the composite Churchill plate experienced three major deformation, magmatic and metamorphic events (M1–M3), associated with sequential accretion of the Meta Incognita microcontinent[186] and the Narsajuaq Arc terrane[187] to the southern margin of the Archaean Rae Craton (FIG. 6).

Accretion of the Meta Incognita microcontinent led to closure of the south-dipping Baffin suture and formation at ~1,915–1,896 Ma (REFS[188,189]) of a north-verging, thin-skinned, thrust-fold belt (Foxe Fold Belt) (FIG. 6) along the southern margin of the Rae Craton on Baffin Island. The Foxe Fold Belt marks the northern extent of penetrative THO deformation. Emplacement of the calc-alkaline granodiorite–tonalite Qikiqtarjuaq plutonic suite[190,191] occurred from ~1,896–1,886 Ma (REF.[189]). This magmatism was accompanied by development of a regional low-P and high-T metamorphic domain (M1) within the Foxe Fold Belt, with cordierite–andalusite assemblages that have yielded P–T estimates of 3.0–4.0 kbar and 550–600 °C (REF.[192]), and regional granulite-facies contact metamorphism dated at ~1,897–1,875 Ma (REFS[193,194]). Subsequent emplacement of the voluminous monzogranite–granodiorite Cumberland batholith at ~1,865–1,845 Ma (REFS[195,196]) is

Prograde
Metamorphic conditions characterized by increasing temperature and (typically) pressure.

Retrogressed
A mineral assemblage that has re-equilibrated (usually partially) on the retrograde path, generally at lower pressure and temperature conditions than the peak assemblage and due to the influx of a hydrous fluid.

attributed to subduction-related magmatic activity[180] or large-scale delamination of lithospheric mantle[197].

Continued convergence between the leading edge of the Churchill plate and crustal domains to the south led to accretion of the Narsajuaq Arc terrane, including the extensive 2,000-Ma Purtuniq ophiolite[186,198] (FIG. 6), and closure of the north-dipping Soper River suture at ~1,845–1,842 Ma (REFS[187,199]). Emplacement of the Cumberland batholith and accretion of the Narsajuaq Arc terrane resulted in granulite-facies metamorphism of the Meta Incognita microcontinent (M2), with pelitic assemblages including high-T garnet–cordierite and leucosome segregations[176]. Peak metamorphism is constrained at 6.0–7.5 kbar and 810–890 °C (REFS[200,201]), and developed during a clockwise P–T cycle[201]. Prograde metamorphism is dated at ~1,862–1,850 Ma, with retrograde partial melt crystallization occurring at ~1,823–1,805 Ma (REF.[201]), indicating regional, long-duration, high-T metamorphism that overlapped with the terminal collision in the THO.

Calc-alkaline tonalite–granodiorite–diorite gneiss from the lower crustal levels of the Narsajuaq Arc terrane, dated between ~1,863 and 1,845 Ma (REFS[177,187]), was intruded by monzodiorite to granite plutons at ~1,842 and 1,820 Ma (REFS[177,187]). The gneiss contains M3 mineral assemblages consistent with granulite-facies conditions that are spatially distinct from M2. P–T estimates range between 6–9 kbar and 800–900 °C (REF.[196]), and M3 metamorphism culminated at ~1,836–1,825 Ma (REF.[177]). Cross-cutting leucogranite dykes are dated between ~1,797 and 1,785 Ma (REF.[177]). As a whole, magmatism in the Narsajuaq Arc terrane records the tectonic evolution from an oceanic island-arc environment to a continental-margin subduction environment, to a continental collision crustal environment with progressive closure of the southern Manikewan Ocean[187].

Terrane accretion in the western segment of the THO is documented to have led to formation of an orogenic plateau that was tectonically and magmatically active for >100 Myr (REFS[182,184]).

Superior units

In the footwall of the north-dipping terminal collisional suture of the THO (Bergeron suture) (FIG. 6), Palaeoproterozoic Superior Craton sedimentary and volcanic sequences were imbricated by south-directed thrust faults. The thrusting was both thin-skinned and in-sequence, and occurred between 1,870 and 1,820 Ma, above a regional basal décollement, forming the Cape Smith thrust-fold belt of northern Quebec[202] (FIG. 6).

Three phases of metamorphism (M4a–c) characterize the progressive syn-orogenic thermal evolution of the basement and cover units that formed the leading edge of the Superior plate. The oldest phase (M4a) is defined by retrogressed eclogite preserved in the Kovik tectonic window (starred locality, FIG. 6), which records P–T conditions of ~25 kbar and 735 °C between 1,831 and 1,820 Ma (REF.[178]), suggesting syn-collisional, deep continental underthrusting. This near-UHP metamorphism was followed by regional M4b greenschist-facies to amphibolite-facies Barrovian-type metamorphism resulting from in-sequence thrusting of cover units along the northern margin of the Superior Craton[203]. During M4b, P–T conditions increased from the front of the thrust belt (foreland) to the back (hinterland) along the exposed base of the Cape Smith belt (FIG. 6) from 6 kbar and 400 °C to 9 kbar and 575 °C, consistent with the interpretation of the thrust belt as a southwards-tapering wedge[196]. M4b is bracketed between 1,820 and 1,815 Ma, and interpreted to be the result of thermal relaxation in the tectonically thickened belt[204].

M4c amphibolite-facies conditions are recorded in recrystallized portions of the underthrust Superior Craton crystalline basement, with P–T conditions increasing from foreland to hinterland from 7 kbar and 585 °C to 10 kbar and 720 °C (REF.[205]). Observations in the Douglas Harbour tectonic window (FIG. 6) reveal that the Superior Craton basement transitions structurally downwards from hydrous to anhydrous rocks. The hydrous rocks are recrystallized Palaeoproterozoic amphibolite-facies rocks that exhibit a foliation broadly sub-parallel to the base of the overlying Cape Smith thrust-fold belt. The anhydrous rocks are Archaean granulite-facies rocks that preserve original high-T deformation fabrics and mineral assemblages. This relationship has been ascribed to water infiltration and reaction during the propagation of the overlying thrust-fold belt during the THO[206].

Re-equilibration of the footwall basement occurred at ~1,815–1,785 Ma (REF.[207]), during and following a renewed period of thrusting. The younger thrust faults re-imbricate the previously thrusted cover units of the Superior Craton[202]. They are thick-skinned, as they also involve the cratonic basement, and collisional in origin, as they can be linked to the main Bergeron collisional suture. The structural and thermal evolution of the Superior units, thus, documents the formation and growth of a southwards-tapering crustal wedge prior to and during continental collision.

Magmatism within the Superior units is restricted to the emplacement of muscovite–biotite–garnet–tourmaline leucogranite dykes and sills dominantly between 1,795 and 1,785 Ma, with a subset as young as 1,758 Ma (REF.[177]). Post-orogenic folding at ~1.76–1.74 Ga contributed to the formation of the structural windows into the Superior Craton basement (Kovik and Douglas Harbour) (FIG. 6). Subsequent slow cooling and exhumation of the north-eastern Arctic Canada segment of the THO is indicated by regional muscovite $^{40}Ar/^{39}Ar$ ages of ~1,690–1,660 Ma (REF.[208]). Both the crustal magmatism and post-collisional folding of the Superior units document the long-term thermal weakening of cratonic units as a consequence of collisional orogenesis.

Comparing ancient and active orogens

Building on the sections above, the similarities and differences between the magmatic and metamorphic rock records of the reviewed orogens are now discussed, using the onset of collision as a common datum (FIG. 2).

Similarities

Common to all the orogenic records are generally extensive periods of pre-collisional magmatism (magenta bars, FIG. 2), with their occurrence and termination assisting in defining the polarity of subduction and onset of continent–continent collision, respectively. Consistent with the magmatic record, pre-collisional metamorphism (where identified) is predominantly of high-T and low-P character (orange bars, FIG. 2).

Each orogen also preserves evidence of syn-collisional to post-collisional 'Barrovian-type' metamorphism (blue to green bars as grade increases, FIG. 2), including crustal melting and leucogranite emplacement (light pink bars, FIG. 2). These similarities are present, despite different configurations of the surrounding plate boundaries and, consequently, forces that were driving the mountain building[209]. The comparable post-collisional metamorphism is likely to be related to the nature of the bounding plates, which are dominantly composed of Archaean to Mesoproterozoic cratons that experienced high-grade metamorphism and dehydration prior to being involved in the respective orogens (India and the Tarim block, Baltica and Laurentia, the Superior and Rae cratons).

As the crust of a mountain belt is thickened, the gravitational potential energy contrast between the range and its surrounding lowlands increases[210–212], and the bounding plates can only support a finite magnitude of this force[213,214]. Therefore, the bounding plate rheology limits the crustal thickness that can be attained within a mountain belt, analogous to the mountains being a 'pressure gauge' for the stresses transmitted through the bounding plates[213]. This concept, and the geologically similar forelands of the analysed orogens, explains the similarity in the estimated past crustal thicknesses (of roughly double normal-thickness crust). Crustal thickness is itself one of the dominant controls on the thermal evolution of mountain belts, and, so, controls the temperatures attained[35,36,215]. Therefore, it is likely that the similar metamorphic conditions reached in the orogens described here are due to similarities in the metamorphic history and, so, rheology of the bounding plates.

Not all collisional mountain belts are flanked by strong cratons. In the present day, those mountain belts that lack bounding cratons have lower crustal thicknesses (<60 km) and less evidence of high-grade metamorphism and crustal melting (such as the mountains of the Balkans, central Mongolia and much of Iran). Therefore, such ranges stand less chance of leaving a substantial imprint in the geological record, following erosion back to normal-thickness crust. This effect leads to an inherent bias in the geological record towards the thicker mountain belts preserving the clearest signs of metamorphism and magmatism, with less known about the more modestly sized (but possibly more plentiful) ancient mountain ranges.

The present-day forces required to continue convergence in the HTO are known to be larger than those provided by 'ridge push' from the Central Indian Ridge on the opposite boundary of the Indian plate[216,217]. The explanation for the continued convergence is that plate boundary forces are transmitted throughout tectonic plates. For example, the resisting forces related to convergence in the HTO are balanced by driving forces from 'ridge push' along the Central Indian and Southeast Indian ridges, and 'slab pull' from the Sumatra subduction zone along the north-eastern margin of the Indo-Australian composite plate[216]. Similar crustal thicknesses in the ancient orogens reviewed herein imply that multiple driving forces positioned around the circumference of significantly sized bounding plates probably also existed for those mountain belts, as none would be possible to sustain by forces from an opposing mid-ocean ridge alone.

A further similarity between the studied mountain belts is their recorded durations of metamorphism, magmatism and deformation following continent–continent collision. Although there is some variability, it is less than a factor of two, which is surprising, considering the differences between them in terms of structural level, preservation bias and wider tectonic framework. The large tracts of geologically similar rocks in the forelands of the belts (for example, India, Baltica, Superior) imply that the end of mountain building is not due to weakening of the foreland. The similarity in mountain building duration is also not due to the mountain ranges becoming too thick to support. If the foreland rheology remains constant, mountain belts will grow to the crustal thickness that can be supported by the bounding plate, then expand laterally and form a plateau[6,213], and this process does not place any limit on the longevity of the mountain belt. Although changes in the distribution of forces on the margins of plates occur over tens to hundreds of millions of years[209], it would be extremely coincidental if such a change occurred roughly the same amount of time after the onset of continent–continent collision in each of these belts.

The present-day HTO can provide a clue to the origins of this broad similarity in mountain belt duration. The locations of lower crustal earthquakes show that, beneath north-west Tibet, the northwards-underthrusting Indian Craton is in proximity to the southwards-underthrusting Tarim block[218]. This geometry is thought to have resulted in India pushing the western end of Tarim, leading to its clockwise rotation[218]. The resulting along-strike gradient in convergence rate between India and Tarim represents a westwards decrease in the total convergence rate across the HTO, which is compensated by the westwards increase in the rate of convergence in the Tien Shan[11,219] (FIG. 3). Continued underthrusting on both margins of the HTO will eventually lead to contact between the Indian Craton and the Tarim block at depth, cessation of shortening across the Himalaya and Tibet, and transferral of total India–Asia convergence (at this longitude) to the Tien Shan or elsewhere.

The timescale for the rigid blocks bounding a mountain belt to come into contact at depth is given by their initial separation and the convergence rate. These quantities will vary between mountain ranges. However, for generic orogen widths and convergence rates, timescales on the order of tens of millions of years would be expected (for example, 1,000 km of separation and a convergence rate of 2 cm per year results in a timescale of 50 Myr). The tens of millions of years durations of mountain building events in the orogens described above might, therefore, be controlled by the time taken for the rigid bounding plates to make contact in the lower crust and their strength to resist further convergence and deformation.

Differences

Some aspects of the rock records diverge following collision. In the HTO, present-day exposure is mostly sedimentary rocks, with a narrow sliver of high-grade metamorphic rocks and associated partial melts exposed in the Greater Himalaya Sequence. In contrast, the CO, GO and SNO expose extensive tracts of high-*P* (10–20 kbar), high-*T* rocks (green bars, FIG. 2), representing deep sections of the overthickened crust[58]. The THO is intermediate between these extremes, exposing high-grade rocks as well as low-grade fold-thrust belts and an ophiolite sequence indicative of relatively shallow preserved levels[198]. Modelling of the thermal structure beneath Tibet, constrained by xenolith-derived *P*–*T*–*t* estimates and spatiotemporal patterns of plateau volcanism[32], predicts an evolution in thermal conditions consistent with *P*–*T* conditions determined in the deeply eroded segments of the CO, GO and SNO[35,36]. This comparison indicates that the different rock records are mainly the result of differences in the exposed structural level (FIG. 1c).

This concept is further highlighted by the records of HP to UHP rocks (purple bars, FIG. 2), interpreted to document deep continental underthrusting, diverging in their relative timing and extent. Relict HP to UHP eclogite assemblages are exposed in the HTO and THO suture zones that formed during the onset of collision[178]. In contrast, the CO preserves UHP assemblages related to both pre and late syn-collisional stages, whereas such records are absent in the GO and the SNO. Factors controlling the exhumation of HP to UHP rocks remain contentious[220], but the preservation of such rocks is clearly affected by structural level, with a notable absence from the deepest studied orogens. Awareness of the role of structural level is important because it skews the ancient orogenic rock record.

Comparison of the orogens discussed above indicates that age is not the dominant factor that controls the present-day surface exposure, as the oldest orogen (the THO) features the second highest structural level. Following erosion, the structural level exposed at the surface is, in part, a function of the thickness of the crust when the mountain belt was active, which is governed by the strength of the bounding plates, as discussed above. The other key factor is the density structure of the entire lithosphere, which, during isostatic equilibration, controls the crustal thickness after erosion to near sea level. The crustal thickness during mountain building, and lithospheric density, therefore, control the distance above the Moho that is eventually exposed at the surface. In addition, any later tectonic or magmatic events can influence the erosion level, such as extension (as occurred late to post-orogenically in the CO, GO and SNO) or magmatic underplating.

Summary and future directions

This Review highlights the broad similarities between five HTO-scale orogens that have occurred within the last 2 Gyr. The similarities are likely due to them all having experienced sustained convergence between strong bounding crustal blocks. However, there is a wide diversity of crustal thicknesses and deformation styles within the world's mountain ranges in the present day, with the HTO being unique in terms of its crustal (and lithospheric) architecture[12,18]. An important avenue for future research should explore the causes and consequences of lateral variations in mountain building processes, for example, along the Alpine-Himalayan belt, which is dominantly more modest in scale than the HTO. Such work will involve synthesizing studies of active deformation with analysis of a diversity of ancient orogens, coupled with consideration of their sedimentological and geochemical records[221–224].

A more complete understanding of the causes, consequences and expressions of the lateral variability in mountain belts will enable more detailed and robust conclusions to be drawn from the rock record, particularly where the record is more fragmentary, such as in the Archaean. Such an ability will be particularly important for studying the early Earth and establishing whether mountain building processes and products have varied over Earth history[225,226].

Published online: 19 October 2021

1. Molnar, P., Boos, W. R. & Battisti, D. S. Orographic controls on climate and paleoclimate of Asia: thermal and mechanical roles for the Tibetan Plateau. *Annu. Rev. Earth Planet. Sci.* **38**, 77–102 (2010).
2. Raymo, M. E. & Ruddiman, W. F. Tectonic forcing of late Cenozoic climate. *Nature* **359**, 117–122 (1992).
3. England, P. & Jackson, J. Uncharted seismic risk. *Nat. Geosci.* **4**, 348–349 (2011).
4. Bilham, R., Gaur, V. K. & Molnar, P. Himalayan seismic hazard. *Science* **293**, 1442–1444 (2001).
5. Hilton, R. G. & West, A. J. Mountains, erosion and the carbon cycle. *Nat. Rev. Earth Environ.* **1**, 284–299 (2020).
6. England, P. & Jackson, J. Active deformation of the continents. *Annu. Rev. Earth Planet. Sci.* **17**, 197–226 (1989).
7. Holland, T. J., Green, E. C. & Powell, R. Melting of peridotites through to granites: a simple thermodynamic model in the system KNCFMASHTOCr. *J. Petrol.* **59**, 881–900 (2018).
8. Kohn, M. J., Engi, M. & Lanari, P. Petrochronology. *Methods Appl. Mineral. Soc. Am. Rev. Mineral. Geochem.* **83**, 575 (2017).
9. Fossen, H., Cavalcante, G. C. G., Pinheiro, R. V. L. & Archanjo, C. J. Deformation–progressive or multiphase? *J. Struct. Geol.* **125**, 82–99 (2019).
10. Hatzfeld, D. & Molnar, P. Comparisons of the kinematics and deep structures of the Zagros and Himalaya and of the Iranian and Tibetan plateaus and geodynamic implications. *Rev. Geophys.* **48**, RG2005 (2010).
11. Zhang, P.-Z. et al. Continuous deformation of the Tibetan Plateau from global positioning system data. *Geology* **32**, 809–812 (2004).
12. Priestley, K., Ho, T. & Mitra, S. in *Himalayan Tectonics: A Modern Synthesis* Vol. 483 (eds Searle, M. P. & Treloar, P. J.) 483–516 (The Geological Society of London, 2019).
13. Nábělek, J. et al. Underplating in the Himalaya-Tibet collision zone revealed by the Hi-CLIMB experiment. *Science* **325**, 1371–1374 (2009).
14. Dewey, J. F., Shackleton, R. M., Chengfa, C. & Yiyin, S. The tectonic evolution of the Tibetan Plateau. *Phil. Trans. R. Soc. Lond. A* **327**, 379–413 (1988).
15. Yin, A. & Harrison, T. M. Geologic evolution of the Himalayan-Tibetan orogen. *Annu. Rev. Earth Planet. Sci.* **28**, 211–280 (2000).
16. Kohn, M. J. Himalayan metamorphism and its tectonic implications. *Annu. Rev. Earth Planet. Sci.* **42**, 381–419 (2014).
17. Mitchell, R. N. et al. The supercontinent cycle. *Nat. Rev. Earth Environ.* **2**, 358–374 (2021).
18. McKenzie, D. & Priestley, K. Speculations on the formation of cratons and cratonic basins. *Earth Planet. Sci. Lett.* **435**, 94–104 (2016).
19. Rowley, D. B. & Currie, B. S. Palaeo-altimetry of the late Eocene to Miocene Lunpola basin, central Tibet. *Nature* **439**, 677–681 (2006).
20. An, W., Hu, X., Garzanti, E., Wang, J. & Liu, Q. New precise dating of the India-Asia collision in the Tibetan Himalaya at 61 Ma. *Geophys. Res. Lett.* **48**, e2020GL090641 (2021).
21. Najman, Y. et al. The Tethyan Himalayan detrital record shows that India–Asia terminal collision occurred by 54 Ma in the Western Himalaya. *Earth Planet. Sci. Lett.* **459**, 301–310 (2017).
22. Green, O. R., Searle, M. P., Corfield, R. I. & Corfield, R. M. Cretaceous-Tertiary carbonate platform evolution and the age of the India-Asia collision along the Ladakh Himalaya (northwest India). *J. Geol.* **116**, 331–353 (2008).
23. St-Onge, M. R., Rayner, N. & Searle, M. P. Zircon age determinations for the Ladakh batholith at Chumathang (Northwest India): implications for the age of the India–Asia collision in the Ladakh Himalaya. *Tectonophysics* **495**, 171–183 (2010).
24. Bouilhol, P., Jagoutz, O., Hanchar, J. M. & Dudàs, F. Ö. Dating the India–Eurasia collision through arc magmatic records. *Earth Planet. Sci. Lett.* **366**, 163–175 (2013).
25. Van Hinsbergen, D. J. et al. Restoration of Cenozoic deformation in Asia and the size of Greater India. *Tectonics* **30**, TC5003 (2011).

26. Weller, O. et al. Quantifying the *P–T–t* conditions of north–south Lhasa terrane accretion: new insight into the pre-Himalayan architecture of the Tibetan plateau. *J. Metamorph. Geol.* **33**, 91–113 (2015).
27. Kapp, P. & DeCelles, P. G. Mesozoic–Cenozoic geological evolution of the Himalayan-Tibetan orogen and working tectonic hypotheses. *Am. J. Sci.* **319**, 159–254 (2019).
28. Kapp, P. et al. Tectonic evolution of the early Mesozoic blueschist-bearing Qiangtang metamorphic belt, central Tibet. *Tectonics* **22**, 1043 (2003).
29. Weller, O. et al. U–Pb zircon geochronology and phase equilibria modelling of a mafic eclogite from the Sumdo complex of south-east Tibet: insights into prograde zircon growth and the assembly of the Tibetan plateau. *Lithos* **262**, 729–741 (2016).
30. Chu, M.-F. et al. Zircon U-Pb and Hf isotope constraints on the Mesozoic tectonics and crustal evolution of southern Tibet. *Geology* **34**, 745–748 (2006).
31. Palin, R. et al. Monazite geochronology and petrology of kyanite- and sillimanite-grade migmatites from the northwestern flank of the eastern Himalayan syntaxis. *Gondwana Res.* **26**, 323–347 (2014).
32. Chung, S.-L. et al. Tibetan tectonic evolution inferred from spatial and temporal variations in post-collisional magmatism. *Earth Sci. Rev.* **68**, 173–196 (2005).
33. Chan, G. H.-N. et al. Probing the basement of southern Tibet: evidence from crustal xenoliths entrained in a Miocene ultrapotassic dyke. *J. Geol. Soc.* **166**, 45–52 (2009).
34. Hacker, B. R. et al. Hot and dry deep crustal xenoliths from Tibet. *Science* **287**, 2463–2466 (2000).
35. Craig, T., Kelemen, P., Hacker, B. & Copley, A. Reconciling geophysical and petrological estimates of the thermal structure of southern Tibet. *Geochem. Geophys. Geosystems* **21**, e2019GC008837 (2020).
36. McKenzie, D. & Priestley, K. The influence of lithospheric thickness variations on continental evolution. *Lithos* **102**, 1–11 (2008).
37. Brown, L. et al. Bright spots, structure, and magmatism in southern Tibet from INDEPTH seismic reflection profiling. *Science* **274**, 1688–1690 (1996).
38. Weller, O., St-Onge, M., Rayner, N., Searle, M. & Waters, D. Miocene magmatism in the Western Nyainqentanglha mountains of southern Tibet: an exhumed bright spot? *Lithos* **245**, 147–160 (2016).
39. Searle, M. P. et al. Age and anatomy of the Gongga Shan batholith, eastern Tibetan Plateau, and its relationship to the active Xianshui-he fault. *Geosphere* **12**, 948–970 (2016).
40. Kapp, P., Taylor, M., Stockli, D. & Ding, L. Development of active low-angle normal fault systems during orogenic collapse: insight from Tibet. *Geology* **36**, 7–10 (2008).
41. Ainscoe, E. et al. Blind thrusting, surface folding, and the development of geological structure in the M_w 6.3 2015 Pishan (China) earthquake. *J. Geophys. Res. Solid Earth* **122**, 9359–9382 (2017).
42. Wittlinger, G. et al. Teleseismic imaging of subducting lithosphere and Moho offsets beneath western Tibet. *Earth Planet. Sci. Lett.* **221**, 117–130 (2004).
43. Martin, A. J. A review of Himalayan stratigraphy, magmatism, and structure. *Gondwana Res.* **49**, 42–80 (2017).
44. Kellett, D. A., Cottle, J. M. & Larson, K. P. in *Himalayan Tectonics: A Modern Synthesis* Vol. 483 (eds Searle, M. P. & Treloar, P. J.) 377–400 (The Geological Society of London, 2019).
45. Waters, D. J. in *Himalayan Tectonics: A Modern Synthesis* Vol. 483 (eds Searle, M. P. & Treloar, P. J.) 325–375 (The Geological Society of London, 2019).
46. DeCelles, P. G., Robinson, D. M. & Zandt, G. Implications of shortening in the Himalayan fold-thrust belt for uplift of the Tibetan Plateau. *Tectonics* **21**, 12-1–12-25 (2002).
47. DeCelles, P. G. et al. Neogene foreland basin deposits, erosional unroofing, and the kinematic history of the Himalayan fold-thrust belt, western Nepal. *GSA Bull.* **110**, 2–21 (1998).
48. Goscombe, B., Gray, D. & Foster, D. A. Metamorphic response to collision in the Central Himalayan Orogen. *Gondwana Res.* **57**, 191–265 (2018).
49. Mottram, C. M., Cottle, J. M. & Kylander-Clark, A. R. C. Campaign-style U-Pb titanite petrochronology: along-strike variations in timing of metamorphism in the Himalayan metamorphic core. *Geosci. Front.* **10**, 827–847 (2019).
50. O'Brien, P. J. in *Himalayan Tectonics: A Modern Synthesis* Vol. 483 (eds Searle, M. P. & Treloar, P. J.) 183–213 (The Geological Society of London, 2019).
51. Weinberg, R. F. Himalayan leucogranites and migmatites: nature, timing and duration of anatexis. *J. Metamorph. Geol.* **34**, 821–843 (2016).
52. Wang, R., Weinberg, R. F., Zhu, D.-C., Hou, Z.-Q. & Yang, Z.-M. The impact of a tear in the subducted Indian plate on the Miocene geology of the Himalayan-Tibetan orogen. *GSA Bull.* https://doi.org/10.1130/B36023.1 (2021).
53. Mottram, C. M. et al. Developing an inverted Barrovian sequence; insights from monazite petrochronology. *Earth Planet. Sci. Lett.* **403**, 418–431 (2014).
54. Larson, K. P., Shrestha, S., Soret, M. & Smit, M. The P-T-t-D evolution of the Mahabharat, east-central Nepal: the out-of-sequence development of the Himalaya. *Geosci. Front.* https://doi.org/10.1016/j.gsf.2020.08.001 (2020).
55. Butler, R. W. H. in *Himalayan Tectonics: A Modern Synthesis* Vol. 483 (eds. Searle, M. P. & Treloar, P. J.) 215–254 (The Geological Society of London, 2019).
56. Booth, A. L., Chamberlain, C. P., Kidd, W. S. F. & Zeitler, P. K. Constraints on the metamorphic evolution of the eastern Himalayan syntaxis from geochronologic and petrologic studies of Namche Barwa. *GSA Bull.* **121**, 385–407 (2009).
57. Beaumont, C., Jamieson, R. A., Nguyen, M. H. & Lee, B. Himalayan tectonics explained by extrusion of a low-viscosity crustal channel coupled to focused surface denudation. *Nature* **414**, 738–742 (2001).
58. Jamieson, R. A. & Beaumont, C. On the origin of orogens. *GSA Bull.* **125**, 1671–1702 (2013).
59. Dahlen, F. A. Critical taper model of fold-and-thrust belts and accretionary wedges. *Annu. Rev. Earth Planet. Sci.* **18**, 55–99 (1990).
60. Copley, A., Avouac, J.-P. & Wernicke, B. P. Evidence for mechanical coupling and strong Indian lower crust beneath southern Tibet. *Nature* **472**, 79–81 (2011).
61. Herman, F. et al. Exhumation, crustal deformation, and thermal structure of the Nepal Himalaya derived from the inversion of thermochronological and thermobarometric data and modeling of the topography. *J. Geophys. Res. Solid Earth* **115**, B06407 (2010).
62. Cottle, J. M., Larson, K. P. & Kellett, D. A. How does the mid-crust accommodate deformation in large, hot collisional orogens? A review of recent research in the Himalayan orogen. *J. Struct. Geol.* **78**, 119–133 (2015).
63. Parsons, A. J. et al. Orogen-parallel deformation of the Himalayan midcrust: insights from structural and magnetic fabric analyses of the Greater Himalayan Sequence, Annapurna-Dhaulagiri Himalaya, central Nepal. *Tectonics* **35**, 2515–2537 (2016).
64. Palin, R. M., Reuber, G. S., White, R. W., Kaus, B. J. P. & Weller, O. M. Subduction metamorphism in the Himalayan ultrahigh-pressure Tso Morari massif: an integrated geodynamic and petrological modelling approach. *Earth Planet. Sci. Lett.* **467**, 108–119 (2017).
65. Gee, D. G., Fossen, H., Henriksen, N. & Higgins, A. K. From the early Paleozoic platforms of Baltica and Laurentia to the Caledonide Orogen of Scandinavia and Greenland. *Episodes* **31**, 44–51 (2008).
66. Dalziel, I. W. D. & Dewey, J. F. in *Fifty Years of the Wilson Cycle Concept in Plate Tectonics* Vol. 470 (eds Wilson, R. W., Houseman, G. A., McCaffrey, K. J. W., Doré, A. G. & Buiter, S. J. H.) 19–38 (The Geological Society of London, 2019).
67. Ramberg, I. B., Bryhni, I., Nottvedt, A. & Rangnes, K. (eds) *The Making of a Land-Geology of Norway* Vol. 624 (Norwegian Geological Association, 2008).
68. Gee, D. G. & Stephens, M. B. Regional context and tectonostratigraphic framework of the early–middle Paleozoic Caledonide orogen, northwestern Sweden. *Geol. Soc. Lond. Mem.* **50**, 481–494 (2020).
69. Hodges, K. V. Crustal Decoupling in collisional orogenesis: examples from the East Greenland Caledonides and Himalaya. *Annu. Rev. Earth Planet. Sci.* **44**, 685–708 (2016).
70. Streule, M. J., Strachan, R. A., Searle, M. P. & Law, R. D. in *Continental Tectonics and Mountain Building: The Legacy of Peach and Horne* Vol. 335 (eds Law, R. D., Butler, R. W. H., Holdsworth, R. E., Krabbendam, M. & Strachan, R. A.) 207–232 (The Geological Society of London, 2010).
71. Gee, D. G. in *Reference Module in Earth Systems and Environmental Sciences* (Elsevier, 2015).
72. Corfu, F., Andersen, T. B. & Gasser, D. in *New Perspectives on the Caledonides of Scandinavia and Related Areas* Vol. 390 (eds. Corfu, F., Gasser, D. & Chew, D. M.) 9–43 (The Geological Society of London, 2014).
73. Higgins, A. K. & Leslie, A. G. Restoring thrusting in the East Greenland Caledonides. *Geology* **28**, 1019–1022 (2000).
74. Gilotti, J. A. & McClelland, W. C. Geometry, kinematics and timing of extensional faulting in the Greenland Caledonides — A synthesis. *Geol. Soc. Am. Mem.* **202**, 251–271 (2008).
75. Gilotti, J. A., Jones, K. A. & Elvevold, S. Caledonian metamorphic patterns in Greenland. *Geol. Soc. Am. Mem.* **202**, 201–225 (2008).
76. Gilotti, J. A. & Elvevold, S. Extensional exhumation of a high-pressure granulite terrane in Payer Land, Greenland Caledonides: structural, petrologic, and geochronologic evidence from metapelites. *Can. J. Earth Sci.* **39**, 1169–1187 (2002).
77. Strachan, R. A. Evidence in north-east Greenland for late Silurian-early Devonian regional extension during the Caledonian orogeny. *Geology* **22**, 913–916 (1994).
78. Collinson, J. D. et al. Paleoproterozoic and Mesoproterozoic sedimentary and volcanic successions in the northern parts of the East Greenland Caledonian orogen and its foreland. *Geol. Soc. Am. Mem.* **202**, 73–98 (2008).
79. White, A. P., Hodges, K. V., Martin, M. W. & Andresen, A. Geologic constraints on middle-crustal behavior during broadly synorogenic extension in the central East Greenland Caledonides. *Int. J. Earth Sci.* **91**, 187–208 (2002).
80. Andresen, A., Rehnström, E. F. & Holte, M. Evidence for simultaneous contraction and extension at different crustal levels during the Caledonian orogeny in NE Greenland. *J. Geol. Soc.* **164**, 869–880 (2007).
81. Kalsbeek, F. et al. Granites and granites in the East Greenland Caledonides. *Geol. Soc. Am. Mem.* **202**, 227–249 (2008).
82. Kalsbeek, F., Jepsen, H. F. & Nutman, A. P. From source migmatites to plutons: tracking the origin of ca. 435 Ma S-type granites in the East Greenland Caledonian orogen. *Lithos* **57**, 1–21 (2001).
83. Strachan, R. A., Martin, M. W. & Friderichsen, J. D. Evidence for contemporaneous yet contrasting styles of granite magmatism during extensional collapse of the northeast Greenland Caledonides. *Tectonics* **20**, 458–473 (2001).
84. Hallett, B. W., McClelland, W. C. & Gilotti, J. A. The timing of strike-slip deformation along the Storstrømmen shear zone, Greenland Caledonides: U–Pb zircon and titanite geochronology. *Geosci. Can.* **41**, 19–45 (2014).
85. Gilotti, J. A., Nutman, A. P. & Brueckner, H. K. Devonian to Carboniferous collision in the Greenland Caledonides: U-Pb zircon and Sm-Nd ages of high-pressure and ultrahigh-pressure metamorphism. *Contrib. Mineral. Petrol.* **148**, 216–235 (2004).
86. Roberts, D., Nordgulen, O. & Melezhik, V. The Uppermost Allochthon in the Scandinavian Caledonides: from a Laurentian ancestry through Taconian orogeny to Scandian crustal growth on Baltica. *Mem. Geol. Soc. Am.* **200**, 357 (2007).
87. Barnes, C. G. et al. Timing of sedimentation, metamorphism, and plutonism in the Helgeland Nappe Complex, north-central Norwegian Caledonides. *Geosphere* **3**, 683–703 (2007).
88. Barnes, C. et al. Ordovician and Silurian magmatism in the Upper Nappe, Uppermost Allochthon, Helgeland Nappe Complex, north-central Norway. *Nor. J. Geol.* **91**, 121–136 (2011).
89. Augland, L. E., Andresen, A., in *New Perspectives on the Caledonides of Scandinavia and Related Areas* Vol. 390 (eds Corfu, F., Gasser, D. & Chew, D. M.) 655–678 (The Geological Society of London, 2014).
90. Oalmann, J. A. G., Barnes, C. G. & Hetherington, C. J. Geology of the island of Ylvingen, Nordland, Norway: evidence for pre-Scandian (~475 Ma) exhumation in the Helgeland Nappe Complex. *Nor. J. Geol.* **91**, 77–99 (2011).
91. Krogh, E. J., Andresen, A., Bryhni, I., Broks, T. M. & Kristensen, S. E. Eclogites and polyphase *P–T* cycling in the Caledonian Uppermost Allochthon in Troms, northern Norway. *J. Metamorph. Geol.* **8**, 289–309 (1990).
92. Corfu, F., Ravna, E. J. K. & Kullerud, K. A Late Ordovician U–Pb age for the Tromsø Nappe eclogites, Uppermost Allochthon of the Scandinavian Caledonides. *Contrib. Mineral. Petrol.* **145**, 502–513 (2003).
93. Janák, M., Ravna, E. J. K. & Kullerud, K. Constraining peak *P–T* conditions in UHP eclogites: calculated phase equilibria in kyanite- and phengite-bearing eclogite of the Tromsø Nappe, Norway. *J. Metamorph. Geol.* **30**, 377–396 (2012).

94. Furnes, H., Dilek, Y. & Pedersen, R. B. Structure, geochemistry, and tectonic evolution of trench-distal backarc oceanic crust in the western Norwegian Caledonides, Solund-Stavfjord ophiolite (Norway). *GSA Bull.* **124**, 1027–1047 (2012).
95. Slagstad, T. & Kirkland, C. L. Timing of collision initiation and location of the Scandian orogenic suture in the Scandinavian Caledonides. *Terra Nova* **30**, 179–188 (2018).
96. Dunning, G. R. & Pedersen, R. B. U/Pb ages of ophiolites and arc-related plutons of the Norwegian Caledonides: implications for the development of Iapetus. *Contrib. Mineral. Petrol.* **98**, 13–23 (1988).
97. Svenningsen, O. M. Onset of seafloor spreading in the Iapetus Ocean at 608 Ma: precise age of the Sarek Dyke Swarm, northern Swedish Caledonides. *Precambrian Res.* **110**, 241–254 (2001).
98. Gee, D. G., Andréasson, P.-G., Li, Y. & Krill, A. Baltoscandian margin, Sveconorwegian crust lost by subduction during Caledonian collisional orogeny. *GFF* **139**, 36–51 (2017).
99. Andréasson, P.-G., Svenningsen, O. M. & Albrecht, L. Dawn of Phanerozoic orogeny in the North Atlantic tract; Evidence from the Seve-Kalak Superterrane, Scandinavian Caledonides. *GFF* **120**, 159–172 (1998).
100. Andréasson, P.-G. et al. Seve terranes of the Kebnekaise Mts., Swedish Caledonides, and their amalgamation, accretion and affinity. *GFF* **140**, 264–291 (2018).
101. Brueckner, H. K., van Roermund, H. L. M. & Pearson, N. J. An Archean(?) to Paleozoic evolution for a garnet peridotite lens with sub-Baltic shield affinity within the Seve Nappe Complex of Jämtland, Sweden, Central Scandinavian Caledonides. *J. Petrol.* **45**, 415–437 (2004).
102. Gilio, M., Clos, F. & van Roermund, H. L. M. The Friningen Garnet Peridotite (central Swedish Caledonides). A good example of the characteristic PTt path of a cold mantle wedge garnet peridotite. *Lithos* **230**, 1–16 (2015).
103. Kjøll, H. J. et al. Timing of breakup and thermal evolution of a pre-Caledonian Neoproterozoic exhumed magma-rich rifted margin. *Tectonics* **38**, 1843–1862 (2019).
104. Corfu, F., Roberts, R. J., Torsvik, T. H., Ashwal, L. D. & Ramsay, D. M. Peri-Gondwanan elements in the Caledonian Nappes of Finnmark, Northern Norway: implications for the paleogeographic framework of the Scandinavian Caledonides. *Am. J. Sci.* **307**, 434–458 (2007).
105. Fassmer, K. et al. Middle Ordovician subduction of continental crust in the Scandinavian Caledonides: an example from Tjeliken, Seve Nappe Complex, Sweden. *Contrib. Mineral. Petrol.* **172**, 103 (2017).
106. Root, D. & Corfu, F. U–Pb geochronology of two discrete Ordovician high-pressure metamorphic events in the Seve Nappe Complex, Scandinavian Caledonides. *Contrib. Mineral. Petrol.* **163**, 769–788 (2012).
107. Fassmer, K. et al. Diachronous collision in the Seve Nappe Complex: evidence from Lu–Hf geochronology of eclogites (Norrbotten, North Sweden). *J. Metamorph. Geol.* **39**, 819– 842 (2021).
108. Klonowska, I., Janák, M., Majka, J., Froitzheim, N. & Kośmińska, K. Eclogite and garnet pyroxenite from Stor Jougdan, Seve Nappe Complex, Sweden: implications for UHP metamorphism of allochthons in the Scandinavian Caledonides. *J. Metamorph. Geol.* **34**, 103–119 (2016).
109. Bukała, M. et al. UHP metamorphism recorded by phengite eclogite from the Caledonides of northern Sweden: *P–T* path and tectonic implications. *J. Metamorph. Geol.* **36**, 547–566 (2018).
110. Lindqvist, J. E. Thrust-related metamorphism in basement windows of the central Scandinavian Caledonides. *J. Geol. Soc.* **147**, 69–80 (1990).
111. Roffeis, C. & Corfu, F. in *New Perspectives on the Caledonides of Scandinavia and Related Areas* Vol. 390 (eds Corfu, F., Gasser, D. & Chew, D. M.) 525–539 (The Geological Society of London, 2014).
112. Austrheim, H. Eclogitization of lower crustal granulites by fluid migration through shear zones. *Earth Planet. Sci. Lett.* **81**, 221–232 (1987).
113. Bhowany, K. et al. Phase equilibria modelling constraints on *P–T* conditions during fluid catalysed conversion of granulite to eclogite in the Bergen Arcs, Norway. *J. Metamorph. Geol.* **36**, 315–342 (2018).
114. Glodny, J., Kühn, A. & Austrheim, H. Geochronology of fluid-induced eclogite and amphibolite facies metamorphic reactions in a subduction–collision system, Bergen Arcs, Norway. *Contrib. Mineral. Petrol.* **156**, 27–48 (2008).
115. Beckman, V. et al. in *New Perspectives on the Caledonides of Scandinavia and Related Areas* Vol. 390 (eds Corfu, F., Gasser, D. & Chew, D. M.) 403–424 (The Geological Society of London, 2014).
116. Krogh, T. E., Kamo, S. L., Robinson, P., Terry, M. P. & Kwok, K. U–Pb zircon geochronology of eclogites from the Scandian Orogen, northern Western Gneiss Region, Norway: 14–20 million years between eclogite crystallization and return to amphibolite-facies conditions. *Can. J. Earth Sci.* **48**, 441–472 (2011).
117. Cuthbert, S. J., Carswell, D. A., Krogh-Ravna, E. J. & Wain, A. Eclogites and eclogites in the Western Gneiss Region, Norwegian Caledonides. *Lithos* **52**, 165–195 (2000).
118. Hacker, B. R. et al. High-temperature deformation during continental-margin subduction & exhumation: the ultrahigh-pressure Western Gneiss Region of Norway. *Tectonophysics* **480**, 149–171 (2010).
119. Austrheim, H., Erambert, M. & Engvik, A. K. Processing of crust in the root of the Caledonian continental collision zone: the role of eclogitization. *Tectonophysics* **273**, 129–153 (1997).
120. Austrheim, H. Fluid and deformation induced metamorphic processes around Moho beneath continent collision zones: examples from the exposed root zone of the Caledonian mountain belt, W-Norway. *Tectonophysics* **609**, 620–635 (2013).
121. Mørk, M. B. E. A gabbro to eclogite transition on Flemsøy, Sunnmøre, western Norway. *Chem. Geol.* **50**, 283–310 (1985).
122. Medaris, L. G., Brueckner, H. K., Cai, Y., Griffin, W. L. & Janák, M. Eclogites in peridotite massifs in the Western Gneiss Region, Scandinavian Caledonides: petrogenesis and comparison with those in the Variscan Moldanubian Zone. *Lithos* **322**, 325–346 (2018).
123. Engvik, A. K., Willemoes-Wissing, B. & Lutro, O. High-temperature, decompressional equilibration of the eclogite facies orogenic root (Western Gneiss Region, Norway). *J. Metamorph. Geol.* **36**, 529–545 (2018).
124. Bender, H., Ring, U., Almqvist, B. S. G., Grasemann, B. & Stephens, M. B. Metamorphic zonation by out-of-sequence thrusting at back-stepping subduction zones: sequential accretion of the caledonian internides, Central Sweden. *Tectonics* **37**, 3545–3576 (2018).
125. Fossen, H. The role of extensional tectonics in the Caledonides of south Norway. *J. Struct. Geol.* **14**, 1033–1046 (1992).
126. Ganzhorn, A. C. et al. Structural, petrological and chemical analysis of syn-kinematic migmatites: insights from the Western Gneiss Region, Norway. *J. Metamorph. Geol.* **32**, 647–673 (2014).
127. Li, Z. X. et al. Assembly, configuration, and break-up history of Rodinia: a synthesis. *Precambrian Res.* **160**, 179–210 (2008).
128. Rivers, T. et al. in *Tectonic Styles in Canada: The Lithoprobe Perspective* Vol. 49 (eds Percival, J. A., Cook, F. A. & Clowes, R. M.) 97–236 (Geological Association of Canada, 2012).
129. Bingen, B. et al. The Sveconorwegian orogeny. *Gondwana Res.* **90**, 273–313 (2021).
130. Möller, C., Andersson, J., Dyck, B. & Antal Lundin, I. Exhumation of an eclogite terrane as a hot migmatitic nappe, Sveconorwegian orogen. *Lithos* **226**, 147–168 (2015).
131. Indares, A. Deciphering the metamorphic architecture and magmatic patterns of large hot orogens: insights from the central Grenville Province. *Gondwana Res.* **80**, 385–409 (2020).
132. Rivers, T. Assembly and preservation of lower, mid, and upper orogenic crust in the Grenville Province — Implications for the evolution of large hot long-duration orogens. *Precambrian Res.* **167**, 237–259 (2008).
133. Rivers, T. Upper-crustal orogenic lid and mid-crustal core complexes: signature of a collapsed orogenic plateau in the hinterland of the Grenville Province. *Can. J. Earth Sci.* **49**, 1–42 (2012).
134. Groulier, P.-A., Indares, A., Dunning, G., Moukhsil, A. & Jenner, G. Syn-orogenic magmatism over 100 m.y. in high crustal levels of the central Grenville Province: characteristics, age and tectonic significance. *Lithos* **312–313**, 128–152 (2018).
135. Cawood, P. A. & Pisarevsky, S. A. Laurentia-Baltica-Amazonia relations during Rodinia assembly. *Precambrian Res.* **292**, 386–397 (2017).
136. Evans, D. A. D. in *Ancient Orogens and Modern Analogues* Vol. 327 (eds Murphy, J. B., Keppie, J. D. & Hynes, A. J.) 371–404 (The Geological Society of London, 2009).
137. Johansson, Å. From Rodinia to Gondwana with the 'SAMBA' model — A distant view from Baltica towards Amazonia and beyond. *Precambrian Res.* **244**, 226–235 (2014).
138. Martin, E. L. et al. The core of Rodinia formed by the juxtaposition of opposed retreating and advancing accretionary orogens. *Earth-Sci. Rev.* **211**, 103413 (2020).
139. Möller, C. & Andersson, J. Metamorphic zoning and behaviour of an underthrusting continental plate. *J. Metamorph. Geol.* **36**, 567–589 (2018).
140. McMenamin, M. A. S. & McMenamin, D. L. S. *The Emergence of Animals: The Cambrian Breakthrough* (Columbia Univ. Press, 1990).
141. Carr, S. D., Easton, R. M., Jamieson, R. A. & Culshaw, N. G. Geologic transect across the Grenville orogen of Ontario and New York. *Can. J. Earth Sci.* **37**, 193–216 (2000).
142. Marsh, J. H. & Kelly, E. D. Petrogenetic relations among titanium-rich minerals in an anatectic high-P mafic granulite. *J. Metamorph. Geol.* **35**, 717–738 (2017).
143. Indares, A. & Dunning, G. Coronitic metagabbro and eclogite from the Grenville Province of western Quebec: interpretation of U–Pb geochronology and metamorphism. *Can. J. Earth Sci.* **34**, 891–901 (1997).
144. Johnson, T. A., Vervoort, J. D., Ramsey, M. J., Southworth, S. & Mulcahy, S. R. Tectonic evolution of the Grenville Orogen in the central appalachians. *Precambrian Res.* **346**, 105740 (2020).
145. Cao, W., Massonne, H.-J. & Liang, X. Partial melting due to breakdown of phengite and amphibole in retrogressed eclogite of deep Precambrian crust: an example from the Algonquin terrane, western Grenville Province, Canada. *Precambrian Res.* **352**, 105965 (2021).
146. Corrigan, D. & Breemen, O.van U–Pb age constraints for the lithotectonic evolution of the Grenville Province along the Mauricie transect, Quebec. *Can. J. Earth Sci.* **34**, 299–316 (1997).
147. Marsh, J. H. & Culshaw, N. G. Timing and conditions of high-pressure metamorphism in the western Grenville Province: constraints from accessory mineral composition and phase equilibrium modeling. *Lithos* **200–201**, 402–417 (2014).
148. Green, A. G. et al. Crustal structure of the Grenville front and adjacent terranes. *Geology* **16**, 788–792 (1988).
149. Gool, J. A. M., van, Rivers, T. & Calon, T. Grenville Front zone, Gagnon terrane, southwestern Labrador: configuration of a midcrustal foreland fold-thrust belt. *Tectonics* **27**, TC1004 (2008).
150. Connelly, J. N. & Heaman, L. M. U/Pb geochronological constraints on the tectonic evolution of the Grenville Province, western Labrador. *Precambrian Res.* **63**, 123–142 (1993).
151. Indares, A., White, R. W. & Powell, R. Phase equilibria modelling of kyanite-bearing anatectic paragneisses from the central Grenville Province. *J. Metamorph. Geol.* **26**, 815–836 (2008).
152. Gower, C. F., Heaman, L. M., Loveridge, W. D., Schärer, U. & Tucker, R. D. Grenvillian magmatism in the eastern Grenville Province, Canada. *Precambrian Res.* **51**, 315–336 (1991).
153. Maity, B. K. & Rivers, T. in *Geological Society of America Abstracts with Programs* Vol. 52 (Geological Society of America, 2020).
154. Stephens, M. B. & Weihed, J. B. *Sweden: Lithotectonic Framework, Tectonic Evolution and Mineral Resources* (The Geological Society, 2020).
155. Stephens, M. B., Wahlgren, C.-H., Weijermars, R. & Cruden, A. R. Left-lateral transpressive deformation and its tectonic implications, Sveconorwegian orogen, Baltic Shield, southwestern Sweden. *Precambrian Res.* **79**, 261–279 (1996).
156. Viola, G., Henderson, I. H. C., Bingen, B. & Hendriks, B. W. H. The Grenvillian–Sveconorwegian orogeny in Fennoscandia: back-thrusting and extensional shearing along the "Mylonite Zone". *Precambrian Res.* **189**, 368–388 (2011).
157. Slagstad, T. et al. The Sveconorwegian orogeny–Reamalgamation of the fragmented southwestern margin of Fennoscandia. *Precambrian Res.* **350**, 105877 (2020).
158. Drüppel, K., Elsäßer, L., Brandt, S. & Gerdes, A. Sveconorwegian mid-crustal ultrahigh-temperature metamorphism in Rogaland, Norway: U–Pb LA-ICP-MS geochronology and pseudosections of sapphirine granulites and associated paragneisses. *J. Petrol.* **54**, 305–350 (2013).

159. Laurent, A. T., Duchene, S., Bingen, B., Bosse, V. & Seydoux-Guillaume, A.-M. Two successive phases of ultrahigh temperature metamorphism in Rogaland, S. Norway: evidence from Y-in-monazite thermometry. *J. Metamorph. Geol.* **36**, 1009–1037 (2018).
160. Söderlund, U., Hellström, F. A. & Kamo, S. L. Geochronology of high-pressure mafic granulite dykes in SW Sweden: tracking the *P–T–t* path of metamorphism using Hf isotopes in zircon and baddeleyite. *J. Metamorph. Geol.* **26**, 539–560 (2008).
161. Bingen, B. et al. Geochronology of high-grade metamorphism in the Sveconorwegian belt, S. Norway: U-Pb, Th-Pb and Re-Os data. *Nor. J. Geol. Geol. Foren.* **88**, 32–42 (2008).
162. Vander Auwera, J. et al. Sveconorwegian massif-type anorthosites and related granitoids result from post-collisional melting of a continental arc root. *Earth Sci. Rev.* **107**, 375–397 (2011).
163. Åreback, H. & Andersson, U. B. Granulite-facies contact metamorphism around the Hakefjorden norite-anorthosite complex, SW Sweden. *Nor. Geol. Tidsskr.* **82**, 29–44 (2002).
164. Söderlund, U., Jarl, L.-G., Persson, P.-O., Stephens, M. B. & Wahlgren, C.-H. Protolith ages and timing of deformation in the eastern, marginal part of the Sveconorwegian orogen, southwestern Sweden. *Precambrian Res.* **94**, 29–48 (1999).
165. Piñán-Llamas, A. P., Andersson, J., Möller, C., Johansson, L. & Hansen, E. Polyphasal foreland-vergent deformation in a deep section of the 1 Ga Sveconorwegian orogen. *Precambrian Res.* **265**, 121–149 (2015).
166. Tual, L., Pinan-Llamas, A. & Möller, C. High-temperature deformation in the basal shear zone of an eclogite-bearing fold nappe, Sveconorwegian orogen, Sweden. *Precambrian Res.* **265**, 104–120 (2015).
167. Tual, L., Pitra, P. & Möller, C. *P–T* evolution of Precambrian eclogite in the Sveconorwegian orogen, SW Sweden. *J. Metamorph. Geol.* **35**, 493–515 (2017).
168. Tual, L., Möller, C. & Whitehouse, M. Tracking the prograde *P–T* path of Precambrian eclogite using Ti-in-quartz and Zr-in-rutile geothermobarometry. *Contrib. Mineral. Petrol.* **173**, 56 (2018).
169. Hansen, E. et al. Partial melting in amphibolites in a deep section of the Sveconorwegian Orogen, SW Sweden. *Lithos* **236**, 27–45 (2015).
170. Beckman, V., Möller, C., Söderlund, U. & Andersson, J. Zircon growth during progressive recrystallization of gabbro to garnet amphibolite, Eastern Segment, Sveconorwegian orogen. *J. Petrol.* **58**, 167–187 (2017).
171. Wahlgren, C.-H., Cruden, A. R. & Stephens, M. B. Kinematics of a major fan-like structure in the eastern part of the Sveconorwegian orogen, Baltic Shield, south-central Sweden. *Precambrian Res.* **70**, 67–91 (1994).
172. Drake, H., Tullborg, E.-L. & Page, L. Distinguished multiple events of fracture mineralisation related to far-field orogenic effects in Paleoproterozoic crystalline rocks, Simpevarp area, SE Sweden. *Lithos* **110**, 37–49 (2009).
173. Söderlund, U. et al. U–Pb baddeleyite ages and Hf, Nd isotope chemistry constraining repeated mafic magmatism in the Fennoscandian Shield from 1.6 to 0.9 Ga. *Contrib. Mineral. Petrol.* **150**, 174 (2005).
174. Hoffman, P. F. United plates of America, the birth of a craton: Early Proterozoic assembly and growth of Laurentia. *Annu. Rev. Earth Planet. Sci.* **16**, 543–603 (1988).
175. Lewry, J. & Stauffer, M. *The Early Proterozoic Trans-Hudson Orogen of North America* (Geological Association of Canada, 1990).
176. St-Onge, M., Wodicka, N. & Ijewliw, O. Polymetamorphic evolution of the Trans-Hudson Orogen, Baffin Island, Canada: integration of petrological, structural and geochronological data. *J. Petrol.* **48**, 271–302 (2007).
177. St-Onge, M. R., Searle, M. P. & Wodicka, N. Trans-Hudson Orogen of North America and Himalaya-Karakoram-Tibetan Orogen of Asia: structural and thermal characteristics of the lower and upper plates. *Tectonics* **25**, TC4006 (2006).
178. Weller, O. & St-Onge, M. Record of modern-style plate tectonics in the Palaeoproterozoic Trans-Hudson orogen. *Nat. Geosci.* **10**, 305–311 (2017).
179. Corrigan, D., Pehrsson, S., Wodicka, N. & De Kemp, E. in *Ancient Orogens and Modern Analogues* Vol. 327 (eds Murphy, J. B., Keppie, J. D. & Hynes, A. J.) 457–479 (The Geological Society of London, 2009).
180. St-Onge, M. R., Van Gool, J. A., Garde, A. A. & Scott, D. J. in *Earth Accretionary Systems in Space and Time* Vol. 318 (eds. Cawood, P. A. & Kroner, A.) 193–235 (The Geological Society of London, 2009).
181. Corrigan, D., Percival, J., Cook, F. & Clowes, R. in *Tectonic Styles in Canada: The Lithoprobe Perspect*ive Vol. 49 (eds Percival, J. A., Cook, F. A. & Clowes, R. M.) 239–284 (Geological Association of Canada, 2012).
182. Dumond, G. Tibetan dichotomy exposed in the Canadian Shield: a lower crustal perspective. *Earth Planet. Sci. Lett.* **544**, 116375 (2020).
183. St-Onge, M. et al. Archean and Paleoproterozoic cratonic rocks of Baffin Island. *Geol. Surv. Can. Bull.* **608**, 1–29 (2020).
184. Regis, D. et al. Post-1.9 Ga evolution of the south Rae craton (Northwest Territories, Canada): a Paleoproterozoic orogenic collapse system. *Precambrian Res.* **355**, 106105 (2021).
185. Darbyshire, F., Bastow, I., Petrescu, L., Gilligan, A. & Thompson, D. A tale of two orogens: crustal processes in the Proterozoic Trans-Hudson and Grenville Orogens, eastern Canada. *Tectonics* **36**, 1633–1659 (2017).
186. St-Onge, M. R., Scott, D. J. & Lucas, S. B. Early partitioning of Quebec: microcontinent formation in the Paleoproterozoic. *Geology* **28**, 323–326 (2000).
187. Dunphy, J. M. & Ludden, J. N. Petrological and geochemical characteristics of a Paleoproterozoic magmatic arc (Narsajuaq terrane, Ungava Orogen, Canada) and comparisons to Superior Province granitoids. *Precambrian Res.* **91**, 109–142 (1998).
188. Wodicka, N., St-Onge, M. R., Corrigan, D., Scott, D. J. & Whalen, J. B. Did a proto-ocean basin form along the southeastern Rae cratonic margin? Evidence from U-Pb geochronology, geochemistry (Sm-Nd and whole-rock), and stratigraphy of the Paleoproterozoic Piling Group, northern Canada. *GSA Bull.* **126**, 1625–1653 (2014).
189. Rayner, N. U-Pb zircon geochronology constraints on timing of plutonism and sedimentary provenance from the Clearwater Fiord-Sylvia Grinnell Lake area, southern Baffin Island, Nunavut. *Geol. Surv. Can. Open File* **8204**, 32 (2017).
190. Sanborn-Barrie, M., Young, M. & Whalen, J. B. Geology, Qikiqtarjuaq, Baffin Island, Nunavut. *Goverment of Canada* https://publications.gc.ca/site/eng/411355/publication.html (2013).
191. Sanborn-Barrie, M., Young, M., Whalen, J., James, D. & St-Onge, M. R. Geology Touak Fiord, Nunavut. *Geological Survey of Canada* https://doi.org/10.4095/289239 (2011).
192. Allan, M. M. & Pattison, D. R. M. Deformation history and metamorphism of a synformal depression, Longstaff Bluff Formation metaturbidite, central Baffin Island, Nunavut (Natural Resources Canada, Geological Survey of Canada, 2003).
193. Gagné, S., Jamieson, R. A., MacKay, R., Wodicka, N. & Corrigan, D. Texture, composition, and age variations in monazite from the lower amphibolite to the granulite facies, Longstaff Bluff Formation, Baffin Island, Canada. *Can. Mineral.* **47**, 847–869 (2009).
194. Berman, R., Sanborn-Barrie, M., Rayner, N. & Whalen, J. The tectonometamorphic evolution of Southampton Island, Nunavut: insight from petrologic modeling and in situ SHRIMP geochronology of multiple episodes of monazite growth. *Precambrian Res.* **232**, 140–166 (2013).
195. Rayner, N. New (2013–2014) UPb geochronological results from northern Hall Peninsula, southern Baffin Island, Nunavut (Canada-Nunavut Geoscience Office, 2015).
196. St-Onge, M. R., Wodicka, N. & Lucas, S. B. Granulite- and amphibolite-facies metamorphism in a convergent-plate-margin setting: synthesis of the Quebec–Baffin segment of the Trans-Hudson orogen. *Can. Mineral.* **38**, 379–398 (2000).
197. Whalen, J. B., Wodicka, N., Taylor, B. E. & Jackson, G. D. Cumberland batholith, Trans-Hudson Orogen, Canada: petrogenesis and implications for Paleoproterozoic crustal and orogenic processes. *Lithos* **117**, 99–118 (2010).
198. Scott, D. J., Helmstaedt, H. & Bickle, M. J. Purtuniq ophiolite, Cape Smith belt, northern Quebec, Canada: a reconstructed section of Early Proterozoic oceanic crust. *Geology* **20**, 173–176 (1992).
199. Scott, D. J. Geology, U–Pb, and Pb–Pb geochronology of the Lake Harbour area, southern Baffin Island: implications for the Paleoproterozoic tectonic evolution of northeastern Laurentia. *Can. J. Earth Sci.* **34**, 140–155 (1997).
200. Skipton, D. R., St-Onge, M. R., Schneider, D. A. & McFarlane, C. R. M. Tectonothermal evolution of the middle crust in the Trans-Hudson Orogen, Baffin Island, Canada: evidence from petrology and monazite geochronology of sillimanite-bearing migmatites. *J. Petrol.* **57**, 1437–1462 (2016).
201. Weller, O. M., Jackson, S., Miller, W. G. R., St-Onge, M. R. & Rayner, N. Quantitative elemental mapping of granulite-facies monazite: textural insights and implications for petrochronology. *J. Metamorph. Geol.* **38**, 853–880 (2020).
202. Lucas, S. B. Structural evolution of the Cape Smith Thrust Belt and the role of out-of-sequence faulting in the thickening of mountain belts. *Tectonics* **8**, 655–676 (1989).
203. Bégin, N. J. Contrasting mineral isograd sequences in metabasites of the Cape Smith Belt, northern Québec, Canada: three new bathograds for mafic rocks. *J. Metamorph. Geol.* **10**, 685–704 (1992).
204. St-Onge, M. & Lucas, S. Evolution of regional metamorphism in the Cape Smith Thrust Belt (northern Quebec, Canada): interaction of tectonic and thermal processes. *J. Metamorph. Geol.* **9**, 515–534 (1991).
205. St-Onge, M. R. & Ijewliw, O. J. Mineral corona formation during high-*P* retrogression of granulitic rocks, Ungava Orogen, Canada. *J. Petrol.* **37**, 553–582 (1996).
206. St-Onge, M. R. & Lucas, S. B. Large-scale fluid infiltration, metasomatism and re-equilibration of Archaean basement granulites during Palaeoproterozoic thrust belt construction, Ungava Orogen, Canada. *J. Metamorph. Geol.* **13**, 509–535 (1995).
207. Scott, D. J. & St-Onge, M. R. Constraints on Pb closure temperature in titanite based on rocks from the Ungava orogen, Canada: implications for U-Pb geochronology and P-T-t path determinations. *Geology* **23**, 1123–1126 (1995).
208. Skipton, D., Schneider, D., Kellett, D. & Joyce, N. in *Summary of Activities* 17–30 (Canada-Nunavut Geoscience Office, 2014).
209. Merdith, A. S. et al. Extending full-plate tectonic models into deep time: linking the Neoproterozoic and the Phanerozoic. *Earth Sci. Rev.* **214**, 103477 (2021).
210. England, P. & McKenzie, D. A thin viscous sheet model for continental deformation. *Geophys. J. Int.* **70**, 295–321 (1982).
211. Artyushkov, E. V. Stresses in the lithosphere caused by crustal thickness inhomogeneities. *J. Geophys. Res.* **78**, 7675–7708 (1973).
212. Flesch, L. M., Haines, A. J. & Holt, W. E. Dynamics of the India-Eurasia collision zone. *J. Geophys. Res. Solid Earth* **106**, 16435–16460 (2001).
213. Molnar, P. & Lyon-Caen, H. Some simple physical aspects of the support, structure, and evolution of mountain belts. *Process. Cont. Lithospheric Deform.* **218**, 179–207 (1988).
214. Copley, A., Boait, F., Hollingsworth, J., Jackson, J. & McKenzie, D. Subparallel thrust and normal faulting in Albania and the roles of gravitational potential energy and rheology contrasts in mountain belts. *J. Geophys. Res. Solid Earth* **114**, B05407 (2009).
215. England, P. & Thompson, A. B. Pressure–temperature–time paths of regional metamorphism I. Heat transfer during the evolution of regions of thickened continental crust. *J. Petrol.* **25**, 894–928 (1984).
216. Copley, A., Avouac, J.-P. & Royer, J.-Y. India-Asia collision and the Cenozoic slowdown of the Indian plate: implications for the forces driving plate motions. *J. Geophys. Res. Solid Earth* **115**, B03410 (2010).
217. Ghosh, A., Holt, W. E., Flesch, L. M. & Haines, A. J. Gravitational potential energy of the Tibetan Plateau and the forces driving the Indian plate. *Geology* **34**, 321–324 (2006).
218. Craig, T. J., Copley, A. & Jackson, J. Thermal and tectonic consequences of India underthrusting Tibet. *Earth Planet. Sci. Lett.* **353–354**, 231–239 (2012).
219. Avouac, J. P., Tapponnier, P., Bai, M., You, H. & Wang, G. Active thrusting and folding along the northern Tien Shan and Late Cenozoic rotation of the Tarim relative to Dzungaria and Kazakhstan. *J. Geophys. Res. Solid Earth* **98**, 6755–6804 (1993).
220. Hacker, B. R. & Gerya, T. V. Paradigms, new and old, for ultrahigh-pressure tectonism. *Tectonophysics* **603**, 79–88 (2013).
221. Govin, G. et al. Timing and mechanism of the rise of the Shillong Plateau in the Himalayan foreland. *Geology* **46**, 279–282 (2018).
222. Clift, P. D. Controls on the erosion of Cenozoic Asia and the flux of clastic sediment to the ocean. *Earth Planet. Sci. Lett.* **241**, 571–580 (2006).

223. France-Lanord, C., Derry, L. & Michard, A. Evolution of the Himalaya since Miocene time: isotopic and sedimentological evidence from the Bengal Fan. *Geol. Soc. Spec. Publ.* **74**, 603–621 (1993).
224. Dyck, B. et al. in *Himalayan Tectonics: A Modern Synthesis* Vol. 483 (eds. Treloar, P. J. & Searle, M. P.) 281–304 (The Geological Society of London, 2019).
225. Pease, V., Percival, J., Smithies, H., Stevens, G. & Van Kranendonk, M. in *When Did Plate Tectonics Begin on Planet Earth?* Vol. 440 (eds. Condie, K. C. & Pease, V.) 199–228 (Geological Society of America, 2008).
226. Cawood, P. A. et al. Geological archive of the onset of plate tectonics. *Phil. Trans. R. Soc. A* **376**, 20170405 (2018).
227. Parsons, A. J., Hosseini, K., Palin, R. M. & Sigloch, K. Geological, geophysical and plate kinematic constraints for models of the India-Asia collision and the post-Triassic central Tethys oceans. *Earth Sci. Rev.* **208**, 103084 (2020).
228. Henriksen, N. *Caledonian Orogen, East Greenland 70°N–82°N: Geological Map of Greenland 1:1 000 000* (Geological Survey of Denmark and Greenland, 2003).
229. Gee, D. G., Kumpulainen, R., Roberts, D., Stephens, M. B. & Zachrisson, E. *Scandinavian Caledonides, Tectonostratigraphic Map, Scale 1:2,000,000* (Sveriges Geologiska Undersokning, 1985).
230. Gee, D. G., Juhlin, C., Pascal, C. & Robinson, P. Collisional Orogeny in the Scandinavian Caledonides (COSC). *GFF* **132**, 29–44 (2010).
231. Gower, C., Ryan, A. & Rivers, T. in *Mid-Proterozoic Laurentia-Baltica* Vol. 38 (eds Gower, C., Rivers, T. & Ryan, A.) 1–20 (Geological Association of Canada, 1990).
232. Weller, O., Dyck, B., St-Onge, M. R., Rayner, N. & Tschirhart, V. Completing the bedrock mapping of southern Baffin Island, Nunavut; plutonic suites and regional stratigraphy. *Summ. Act.* **2015**, 33–48 (2015).

Acknowledgements
The authors thank P.-G. Andréasson and J. Andersson for discussion. This is NRCan contribution no. 20210115.

Author contributions
All authors contributed to the manuscript preparation and discussion. O.M.W. led the Himalaya-Tibet orogen section, R.S. the Greenland Caledonian orogen, C.M. the Scandinavian Caledonian orogen, T.R. the Grenville orogen, C.M. the Sveconorwegian orogen, M.R.S-O. the Trans-Hudson orogen and A.C. the comparison of the orogens. C.M.M. led figure drafting.

Competing interests
The authors declare no competing interests.

Peer review information
Nature Reviews Earth & Environment thanks V. Pease, M. Bickford and A. Collins for their contribution to the peer review of this work.

Publisher's note
Springer Nature remains neutral with regard to jurisdictional claims in published maps and institutional affiliations.